SANDIA REPORT

SAND2010-4687
Unlimited Release
Printed July 2010

Initial inclusion of thermodynamic considerations in Kayenta

T.J. Fuller, R.M. Brannon, O.E. Strack, J.E. Bishop

Prepared by
Sandia National Laboratories
Albuquerque, New Mexico 87185 and Livermore, California 94550

Sandia National Laboratories is a multi-program laboratory managed and operated by
Sandia Corporation, a wholly owned subsidiary of Lockheed Martin Corporation,
for the U.S. Department of Energy's National Nuclear Security Administration
under contract DE-AC04-94AL85000.

Sandia National Laboratories

Issued by Sandia National Laboratories, operated for the United States Department of Energy by Sandia Corporation.

Available to DOE and DOE contractors from
U.S. Department of Energy
Office of Scientific and Technical Information
P.O. Box 62
Oak Ridge, TN 37831

Telephone: (865) 576-8401
Facsimile: (865) 576-5728
E-Mail: reports@adonis.osti.gov
Online ordering: http://www.osti.gov/bridge

Available to the public from
U.S. Department of Commerce
National Technical Information Service
5285 Port Royal Rd
Springfield, VA 22161

Telephone: (800) 553-6847
Facsimile: (703) 605-6900
E-Mail: orders@ntis.fedworld.gov
Online ordering: http://www.ntis.gov/help/ordermethods.asp?loc=7-4-0#online

SAND2010-4687
Unlimited Release
Printed July 2010

Initial inclusion of thermodynamic considerations in Kayenta

T.J. Fuller
University of Utah
Mechanical Engineering Department
50 South Central Campus Drive
Salt Lake City, UT 84112

J.E. Bishop
Sandia National Laboratories
Comp Struct Mech & Apps
PO Box 5800
Albuquerque, NM 87185-0372

R.M. Brannon
University of Utah
Mechanical Engineering Department
50 South Central Campus Drive
Salt Lake City, UT 84112

O.E. Strack
Sandia National Laboratories
Computational Shock & Multiphysics
PO Box 5800
Albuquerque, NM 87185-0378

Abstract

A persistent challenge in simulating damage of natural geological materials, as well as rock-like engineered materials, is the development of efficient and accurate constitutive models. The common feature for these brittle and quasi-brittle materials are the presence of flaws

such as porosity and network of microcracks. The desired models need to be able to predict the material responses over a wide range of porosities and strain rate. Kayenta [1] (formerly called the Sandia GeoModel) is a unified general-purpose constitutive model that strikes a balance between first-principles micromechanics and phenomenological or semi-empirical modeling strategies. However, despite its sophistication and ability to reduce to several classical plasticity theories, Kayenta is incapable of modeling deformation of ductile materials in which deformation is dominated by dislocation generation and movement which can lead to significant heating. This stems from Kayenta's roots as a geological model, where heating due to inelastic deformation is often neglected or presumed to be incorporated implicitly through the elastic moduli.

The sophistication of Kayenta and its large set of extensive features, however, make Kayenta an attractive candidate model to which thermal effects can be added. This report outlines the initial work in doing just that, extending the capabilities of Kayenta to include deformation of ductile materials, for which thermal effects cannot be neglected.

Thermal effects are included based on an assumption of adiabatic loading by computing the bulk and thermal responses of the material with the Kerley Mie-Grüneisen equation of state and adjusting the yield surface according to the updated thermal state. This new version of Kayenta, referred to as Thermo-Kayenta throughout this report, is capable of reducing to classical Johnson-Cook plasticity in special case single element simulations and has been used to obtain reasonable results in more complicated Taylor impact simulations in LS-Dyna.

Despite these successes, however, Thermo-Kayenta requires additional refinement for it to be consistent in the thermodynamic sense and for it to be considered superior to other, more mature thermoplastic models. The initial thermal development, results, and required refinements are all detailed in the following report.

Acknowledgment

Funding for this work was provided by the Project Manager for the Heavy Brigade Combat Team (PM HBCT, Mr. John Rowe), and is gratefully acknowledged.

Contents

List of Figures

List of Tables

Chapter 1

Introduction

As explained in the Sandia Kayenta user's guide [1, 2], Kayenta (formerly the GeoModel) is a general purpose phenomenological plasticity model developed for use with geological and rock-like engineering materials. In these materials, inelastic deformation is most commonly dominated by the collapse of microscale pores and the growth of microcracks and microcrack networks. Another common feature in these materials is that heating due to inelastic deformation is often neglected or presumed to be incorporated implicitly through the elastic response for adiabatic loading. In this sense, early releases of Kayenta used a purely mechanical equation of state.

Inelastic deformation in metals, on the other hand, is dominated by dislocation generation and movement which can lead to significant heating when subjected to large and high rate deformations [3]. Thus, except for certain restricted classes of deformation, Kayenta is not adequate for predicting material response to general deformation when thermal considerations are not negligible.

This report outlines the initial modifications that have been made to Kayenta to include thermal response due to deformation in accordance with the first and second laws of thermodynamics. Currently, the thermal version of Kayenta, called Thermo-Kayenta throughout this report, can now be demonstrated to reproduce single-element response curves for the Johnson-Cook thermoplasticity model [4] with the Mie-Grüneissen equation of state under strain-controlled compression, pure shear, and uniaxial strain.

This report continues as outlined:

Chapter 2 Elements of Thermomechanics Overview of thermomechanics for thermoelastic and thermoplastic solids.

Chapter 3 Constitutive Models for Thermoplastic Materials Brief discussion of Kayenta, Johnson-Cook plasticity, and the Mie-Grüneisen equation of state.

Chapter 4 Incorporating Thermal Effects in Kayenta: Initial Development Discussion of the initial incorporation of thermodynamics in Thermo-Kayenta.

Chapter 5 Incorporating Thermal Effects in Kayenta: Solution Scheme Discussion of the role of thermodynamics in the current version of Thermo-Kayenta. Installation

instructions for codes in which Kayenta is already installed including a description of the additional subroutines and functions in Thermo-Kayenta.

Chapter 6 Incorporating Thermal Effects in Kayenta: Verification of Results Comparison of the initial thermal capabilities of Thermo-Kayenta with thermoelasticity theory and classical Johnson-Cook plasticity as implemented in ALEGRA.

Chapter 7 Conclusion Concluding remarks.

Chapter 2

Elements of Thermomechanics

The conservation laws developed in the discipline of classical thermomechanics form the basis on which all other physical laws of continuum mechanics are derived. As such, a review of classical thermomechanics is an appropriate starting point for the topics considered in later chapters. Rather than provide a comprehensive overview of the discipline, only those key concepts essential to understanding later material will be considered. For the reader comfortable with the discipline of classical thermomechanics, in particular, its relationship to thermoelasticity and thermoplasticity, this chapter can be skipped without loss of continuity. For a more detailed treatise on classical thermomechanics, the reader may consult such seminal works as *An introduction to the mechanics of a continuous medium* by Malvern [5] or *The non-linear field theories of mechanics* by Truesdell [6].

2.1 Notation and Tensor Representation

Focusing on applications in mechanics, first, second, and fourth-rank tensors are $\mathbb{R}^3$. Components of tensors in $\mathbb{R}^3$ are defined relative to an orthonormal basis $(\mathbf{e}_1, \mathbf{e}_2, \mathbf{e}_3)$ so that $\boldsymbol{a} = a_i \mathbf{e}_i$, $\boldsymbol{A} = A_{ij} \mathbf{e}_i \mathbf{e}_j$, and $\mathbb{A} = A_{ijkl} \mathbf{e}_i \mathbf{e}_j \mathbf{e}_k \mathbf{e}_l$, where implied summation is assumed from 1 - 3. Additionally, second and fourth-rank tensors are presumed symmetric and minor symmetric, respectively, and thus are also equivalently cast as first and symmetric second-rank tensors in $\mathbb{R}^6$ [7]. Components of tensors in $\mathbb{R}^6$ are defined relative to the orthonormal basis $(\mathbf{E}_1, \mathbf{E}_2, \ldots, \mathbf{E}_6)$, thus $\boldsymbol{A} = A_i \mathbf{E}_i$ and $\mathbb{A} = A_{ij} \mathbf{E}_i \mathbf{E}_j$, with implied summation from 1 - 6. The $\mathbf{e}_i$ and $\mathbf{E}_i$ are related by

$$
\begin{aligned}
\mathbf{E}_i &= \mathbf{e}_i \mathbf{e}_i, \quad i = 1, 2, 3, \\
\mathbf{E}_4 &= \frac{1}{\sqrt{2}} \left(\mathbf{e}_1 \mathbf{e}_2 + \mathbf{e}_2 \mathbf{e}_1 \right), \\
\mathbf{E}_5 &= \frac{1}{\sqrt{2}} \left(\mathbf{e}_2 \mathbf{e}_3 + \mathbf{e}_3 \mathbf{e}_2 \right), \\
\mathbf{E}_6 &= \frac{1}{\sqrt{2}} \left(\mathbf{e}_3 \mathbf{e}_1 + \mathbf{e}_1 \mathbf{e}_3 \right).
\end{aligned}
\tag{2.1}
$$

In the above, adjacent basis tensors represent dyads. A raised dot $\bullet$ between tensor arguments represents the inner product of a pair of basis tensors, e.g., $\mathbf{e}_i \bullet \mathbf{e}_j = \delta_{ij}$, where

δ_{ij} is the Kronecker delta, $\boldsymbol{a}\bullet\boldsymbol{b} = a_i b_j \mathbf{e}_i \bullet \mathbf{e}_j = a_i b_i$, $\boldsymbol{A}\colon\boldsymbol{B} = A_{ij}B_{ij}$, etc. Linear mapping, composition, and inner product of tensors of arbitrary rank are thus constructed by the appropriate number of raised dots between arguments.

The norm of a tensor $\mathcal{A}$ is denoted $\|\mathcal{A}\|$ and is defined relative to the orthonormal Euclidean basis is

$$\|\mathcal{A}\|^2 = \sum_{i,j,\ldots,m=1}^{n} \mathcal{A}_{ij\ldots m}\mathcal{A}_{ij\ldots m}, \tag{2.2}$$

where $n = 3$ or 6 if $\mathcal{A} \in \mathbb{R}^3$ or $\mathbb{R}^6$, respectively.

2.2 Conservation Laws in Thermomechanics

Given a conserved quantity contained in an enclosed domain Ω, the rate of change of that quantity must be equal to the sum of the production of the quantity within the domain and the flux of the quantity through the boundary of the domain $\partial\Omega$. Mathematically, conservation laws can be expressed in the following general form

$$\frac{d}{dt}\int_\Omega f(\boldsymbol{x},t)dV = \int_{\partial\Omega} f(\boldsymbol{x},t)\left(v_n(\boldsymbol{x},t) - \boldsymbol{v}(\boldsymbol{x},t)\bullet\boldsymbol{n}(\boldsymbol{x},t)\right)dA + \int_{\partial\Omega} g(\boldsymbol{x},t)dA + \int_\Omega h(\boldsymbol{x},t)dV \tag{2.3}$$

where f is a scalar, vector, or tensor valued conserved quantity, v_n is the normal velocity of the boundary $\partial\Omega$, $\boldsymbol{v}$ is the material velocity, $\boldsymbol{n}$ is the outward unit normal to $\partial\Omega$, g is the surface source of f, and h is the volume source of f, respectively.

Using Eq. (2.3), it can be shown that the conservation of mass, momentum, and energy can be written in local form as

$$\dot{\rho} + \rho\overrightarrow{\nabla}\bullet\boldsymbol{v} = 0 \tag{2.4}$$

$$\overrightarrow{\nabla}\bullet\boldsymbol{\sigma} + \rho\boldsymbol{b} = \rho\boldsymbol{a} \tag{2.5}$$

$$\dot{u} - J\boldsymbol{\sigma}\colon\boldsymbol{d} + J\overrightarrow{\nabla}\bullet\boldsymbol{q} - \rho_0 r = 0 \tag{2.6}$$

where ρ is the material density, $\boldsymbol{\sigma}$ is the Cauchy stress, $\boldsymbol{b}$ is the body force per unit mass, $\boldsymbol{a}$ is the material acceleration, u is the internal energy per unit reference volume, $\boldsymbol{d}$ is the symmetric part of the velocity gradient, J is determinant of the deformation gradient $\boldsymbol{F}$, $\boldsymbol{q}$ is the heat flux vector, and r is the energy production per unit mass. For shock loading, Eq. (2.3) continues to apply and leads to additional Rankine-Hugoniot jump conditions that supplement the above local differential equations [8].

2.3 Entropy and the Second Law of Thermodynamics

The internal energy is commonly regarded as a state function of the other state variables; the general form of this function is restricted by the second law of thermodynamics. For any reversible process, the integral of the heat divided by the temperature is zero over any cycle closed in the thermodynamic state variables.

$$\oint \frac{đQ}{\theta} = 0 \tag{2.7}$$

Thus, even though the heat increment $đQ$ is an inexact differential, dividing it by the temperature θ produces an exact differential in reversible loading. Accordingly, there must exist a state variable, S, such that

$$dS = \frac{đQ}{\theta} \tag{2.8}$$

where S is the total entropy of the system. It is established experimentally that the entropy change for isolated ($Q = 0$) systems is never negative and reaches its maximum at equilibrium. This experimental fact is known as the *second law of thermodynamics*. For non-isolated systems, the entropy change for the system and its surroundings is always non-negative. Mathematically, we can write the second law as

$$\dot{S} = \dot{S}_{\text{sys}} + \dot{S}_{\text{env}} \geq 0 \tag{2.9}$$

Where $\dot{S}_{\text{sys}}$ and $\dot{S}_{\text{env}}$ are the change in entropy of the system and the surrounding environment, respectively. Moreover, entropy is an intrinsic quantity thus implying existence of a specific entropy, s.

2.3.1 The Clausius-Duhem Inequality

Revising the balance law in Eq. (2.3) to allow for imbalance, the second law of thermodynamics can be written

$$\frac{d}{dt}\int_\Omega \rho s dV \geq \int_{\partial\Omega} \rho s \left(v_n(\boldsymbol{x},t) - \boldsymbol{v}(\boldsymbol{x},t)\bullet\boldsymbol{n}(\boldsymbol{x},t)\right) dA - \int_{\partial\Omega} \frac{\boldsymbol{q}\bullet\boldsymbol{n}}{\theta} dA + \int_{\partial\Omega} \frac{\rho r}{\theta} dV \tag{2.10}$$

In local form, Eq. (2.10) becomes

$$\rho_0 \dot{s} \geq -J\overrightarrow{\nabla}\bullet\left(\frac{\boldsymbol{q}}{\theta}\right) + \rho_0 \frac{r}{\theta} \tag{2.11}$$

which is known as the Clausius-Duhem inequality or the entropy inequality.

2.4 Thermoelasticity and Consequences of the Second Law of Thermodynamics

Expanding the first term on the right hand side of Eq. (2.11), the Clausius-Duhem inequality becomes

$$\rho_0 \dot{s} \geq -\frac{J}{\theta}\vec{\nabla}\bullet\boldsymbol{q} + \frac{J}{\theta^2}\boldsymbol{q}\bullet\vec{\nabla}\theta + \rho_0\frac{r}{\theta} \tag{2.12}$$

Substituting the balance of energy, Eq. (2.6), into Eq. (2.12), the Clausius-Duhem inequality may be written as

$$\rho_0\theta\dot{s} \geq \dot{u} - J\boldsymbol{\sigma}\!:\!\boldsymbol{d} + \frac{J}{\theta}\boldsymbol{q}\bullet\vec{\nabla}\theta \tag{2.13}$$

Assuming that $\theta > 0$, the Clausius-Duhem inequality may also be written as a sum of internally dissipative and heat conductive parts

$$\mathcal{D} + \mathcal{F} \geq 0 \tag{2.14}$$

where the internally dissipative part $\mathcal{D}$ is given by

$$\mathcal{D} = J\boldsymbol{\sigma}\!:\!\boldsymbol{d} + \rho_0\theta\dot{s} - \dot{u} \tag{2.15}$$

and the heat conductive part by

$$\mathcal{F} = -\frac{1}{\rho\theta}\boldsymbol{q}\bullet\vec{\nabla}\theta \tag{2.16}$$

For large deformations, where $\boldsymbol{d}$ does not appropriately approximate a true rate of strain, it is necessary to introduce alternative conjugate stress and deformation measures, $\boldsymbol{\mathcal{P}}$, $\boldsymbol{\mathcal{V}}$, such that the stress power

$$J\boldsymbol{\sigma}\!:\!\boldsymbol{d} = \boldsymbol{\mathcal{P}}\!:\!\dot{\boldsymbol{\mathcal{V}}} \tag{2.17}$$

where $\boldsymbol{\mathcal{V}}$ is the elastic strain, and $\boldsymbol{\mathcal{P}}$ is the work conjugate stress. If, for example, the strain is Eulerian logarithmic, then $\boldsymbol{\mathcal{P}}$ is the Kirchhoff stress for proportional loading[1], or, if the strain is the Green-Lagrange then $\boldsymbol{\mathcal{P}}$ is the second Piola-Kirchhoff stress. For the remainder of this dissertation, we choose $\boldsymbol{\mathcal{P}}$ to be the Kirchhoff stress $\boldsymbol{\tau} = J\boldsymbol{\sigma}$ (and, thus, $\boldsymbol{\mathcal{V}}$ is understood to be the Eulerian logarithmic strain $\boldsymbol{\varepsilon}$). Though we have chosen to represent $\boldsymbol{\mathcal{P}}$ and $\boldsymbol{\mathcal{V}}$ as outlined, any other conjugate stress/strain pair would be equally appropriate in the following analysis.

Using Eq. (2.17) and the chosen stress and strain measures, Eq. (2.15) becomes

$$\mathcal{D} = \boldsymbol{\tau}\!:\!\dot{\boldsymbol{\varepsilon}} + \rho_0\theta\dot{s} - \dot{u} \tag{2.18}$$

In thermoelasticity it is presumed that the internal energy is a function of the deformation through the strain tensor and the entropy. In this case, using the chain rule of differentiation,

$$\dot{u} = \frac{\partial u}{\partial \boldsymbol{\varepsilon}}\!:\!\dot{\boldsymbol{\varepsilon}} + \frac{\partial u}{\partial s}\dot{s}$$

[1]We define proportional loading as one for which the principal directions of the reference stretch are stationary, otherwise, the Kirchhoff stress is not generally conjugate to the logarithmic strain [9].

so that Eq. (2.18) can be written

$$\mathcal{D} = \left(\boldsymbol{\tau} - \frac{\partial u}{\partial \boldsymbol{\varepsilon}} \right) \vdots \dot{\boldsymbol{\varepsilon}} + \left(\rho_0 \theta - \frac{\partial u}{\partial s} \right) \dot{s} \tag{2.19}$$

In thermoelastic cases where the stress and temperature are regarded as functions of the deformation and entropy, and that dissipation does not depend on $\dot{\boldsymbol{\varepsilon}}$ or $\dot{s}$, Eq. (2.19) implies that

$$\begin{aligned} \boldsymbol{\tau} &= \frac{\partial u}{\partial \boldsymbol{\varepsilon}} \\ \theta &= \frac{1}{\rho_0} \frac{\partial u}{\partial s} \end{aligned} \tag{2.20}$$

and

$$-\frac{1}{\theta} \boldsymbol{q} \bullet \vec{\nabla} \theta \geq 0 \tag{2.21}$$

Eq. (2.21) implies that, because $\theta > 0$, heat flows in a direction of decreasing temperature. For elastic materials in which the stress is directly derivable from a strain energy potential as described, the material is said to be "hyperelastic". [2]

Using Eq. (2.20), the balance of energy in Eq. (2.6) for thermoelastic materials can be expressed as

$$\rho_0 \theta \dot{s} = -J \vec{\nabla} \bullet \boldsymbol{q} + \rho_0 r \tag{2.22}$$

In other words, the only source of entropy production is from an internal heat source or flow of heat through conduction. This situation is distinguished from plasticity which allows for entropy production through dissipation.

Using the conjugate relations in Eq. (2.20), the rates of stress and temperature are given by

$$\begin{aligned} \dot{\boldsymbol{\tau}} &= \frac{\partial^2 u}{\partial \boldsymbol{\varepsilon} \partial \boldsymbol{\varepsilon}} \vdots \dot{\boldsymbol{\varepsilon}} + \frac{\partial^2 u}{\partial \boldsymbol{\varepsilon} \partial s} \dot{s} \\ \dot{\theta} &= \frac{1}{\rho_0} \frac{\partial^2 u}{\partial s^2} \dot{s} + \frac{1}{\rho_0} \frac{\partial^2 u}{\partial s \partial \boldsymbol{\varepsilon}} \vdots \dot{\boldsymbol{\varepsilon}} \end{aligned} \tag{2.23}$$

Using the following Maxwell and Gibbs relations,

$$\frac{1}{\rho_0} \frac{\partial^2 u}{\partial s^2} = \frac{\partial \theta}{\partial s} = \frac{\theta}{c_v}, \quad \frac{\partial^2 u}{\partial \boldsymbol{\varepsilon} \partial s} = \frac{\partial \boldsymbol{\tau}}{\partial s} = -\rho_0 \theta \boldsymbol{\Gamma}, \quad \frac{\partial^2 u}{\partial \boldsymbol{\varepsilon} \partial \boldsymbol{\varepsilon}} = \mathbb{C}_s \tag{2.24}$$

where $\mathbb{C}_s$ is the isentropic elastic stiffness, $\boldsymbol{\Gamma}$ is the Grüneisen tensor, and c_v is the specific heat at constant volume, Eq. (2.23) can be written in terms of measurable quantities

$$\begin{aligned} \dot{\boldsymbol{\tau}} &= \mathbb{C}_s \vdots \dot{\boldsymbol{\varepsilon}} - \rho_0 \theta \boldsymbol{\Gamma} \dot{s} \\ \dot{\theta} &= \frac{\theta}{c_v} \dot{s} - \theta \boldsymbol{\Gamma} \vdots \dot{\boldsymbol{\varepsilon}} \end{aligned} \tag{2.25}$$

[2] The term "hyperelasticity", sometimes also referred to as "Green" elasticity, refers to the form of elasticity pioneered by Green in which the stress is derivable as the strain gradient of an elastic energy potential. In contrast, "hypoelastic" elastic models are those in which the stress is *not* directly derivable from a strain energy potential, see [6].

For an adiabatically loaded thermoelastic material, since $\dot{s} = 0$, the stress and temperature rates can be found from Eq. (2.25)

$$\begin{aligned} \dot{\boldsymbol{\tau}} &= \mathbb{C}_s \vdots \dot{\boldsymbol{\varepsilon}} \\ \dot{\theta} &= -\theta \boldsymbol{\Gamma} \vdots \dot{\boldsymbol{\varepsilon}} \end{aligned} \tag{2.26}$$

For isothermal loading, Eq. (2.25) is

$$\begin{aligned} \dot{\boldsymbol{\tau}} &= (\mathbb{C}_s - \rho_0 \theta c_v \boldsymbol{\Gamma}\boldsymbol{\Gamma}) \vdots \dot{\boldsymbol{\varepsilon}} = \mathbb{C} \vdots \dot{\boldsymbol{\varepsilon}} \\ \dot{s} &= c_v \boldsymbol{\Gamma} \vdots \dot{\boldsymbol{\varepsilon}} \end{aligned} \tag{2.27}$$

where $\mathbb{C}$ is the isothermal elastic stiffness.

2.5 Thermoplasticity

2.5.1 Conservation Laws for Thermoplastic Materials

For thermoplastic materials, the internal energy depends on elastic strain, entropy, and a set of internal variables that evolve with plastic loading. The stress is allowed to reach a limiting value and entropy is produced not only through heat sources and heat conduction but also through dissipation. The rate of change of internal energy can be expressed as

$$\dot{u} = \frac{\partial u}{\partial \boldsymbol{\varepsilon}^{\mathrm{e}}} \vdots \dot{\boldsymbol{\varepsilon}}^{\mathrm{e}} + \frac{\partial u}{\partial s} \dot{s} + \sum_{k=1}^{n} \frac{\partial u}{\partial q_k} \dot{q}_k \tag{2.28}$$

where $\dot{\boldsymbol{\varepsilon}}^{\mathrm{e}}$ is the rate of elastic strain, q_k are the internal variables that change only with dissipation, and n is the number of internal state variables for the thermoplastic material. Using Eq. (2.28), the dissipation inequality for thermoplastic materials may now be written as

$$\mathcal{D} = \left(\boldsymbol{\tau} - \frac{\partial u}{\partial \boldsymbol{\varepsilon}^{\mathrm{e}}} \right) \vdots \dot{\boldsymbol{\varepsilon}}^{\mathrm{e}} + \left(\rho_0 \theta - \frac{\partial u}{\partial s} \right) \dot{s} - \sum_{k=1}^{n} \psi_k \dot{q}_k + \boldsymbol{\tau} \vdots \dot{\boldsymbol{\varepsilon}}^{\mathrm{p}} \tag{2.29}$$

This form of the dissipation equality is similar to that in Wright [10] and Rosakis, et al. [11], except we have chosen to use the internal energy whereas Wright and Rosakis worked with the Gibbs energy. Note that the dissipation inequality for the thermoplastic material is identical to that of the thermoelastic material in Eq. (2.19) with the addition of the last two terms on the right hand side associated with dissipation. The quantities ψ_k that appear in Eq. (2.29) are work conjugate to the internal state variables and are defined as

$$\psi_k = \frac{\partial u}{\partial q_k} \tag{2.30}$$

We now assume that the temperature gradient does not depend on the rates of strain, entropy, or internal state variables. Then, the entropy inequality for a thermoplastic material can be

expressed as

$$\begin{aligned} \boldsymbol{\tau} &= \frac{\partial u}{\partial \boldsymbol{\varepsilon}^{\mathrm{e}}}, \quad \theta = \frac{1}{\rho_0}\frac{\partial u}{\partial s} \\ \boldsymbol{\tau} \mathbin{:} \dot{\boldsymbol{\varepsilon}}^{\mathrm{p}} - \sum_{k=1}^{n} \psi_k \dot{q}_k &\geq 0 \\ -\frac{1}{\theta}\boldsymbol{q} \cdot \overrightarrow{\nabla}\theta &\geq 0 \end{aligned} \tag{2.31}$$

and the balance of energy as

$$\rho_0 \theta \dot{s} = -J\overrightarrow{\nabla} \cdot \boldsymbol{q} + \rho_0 r + \boldsymbol{\tau} \mathbin{:} \dot{\boldsymbol{\varepsilon}}^{\mathrm{p}} + \sum_{k=1}^{n} \psi_k \dot{q}_k \tag{2.32}$$

2.5.2 Plastic Yield

In plasticity theory, for a given temperature and state of internal variables, the stress in the material is allowed to reach a limiting value, above which plastic deformation will occur. This threshold is defined by a scalar-valued function of stress, temperature, and internal state variables, known as the yield function, f. The yield criterion is expressed mathematically as

$$f(\boldsymbol{\sigma}, \theta, q_k) = 0 \tag{2.33}$$

The yield surface is the set of all stress states satisfying this yield criterion. Elastic states correspond to

$$f(\boldsymbol{\sigma}, \theta, q_k) < 0 \tag{2.34}$$

and plastic states, according to classical rate-independent theories of plasticity, correspond to

$$f(\boldsymbol{\sigma}, \theta, q_k) = 0 \tag{2.35}$$

Viscous, or rate dependent, theories of plasticity, allow the stress state to lie outside of the yield surface and will not be considered in this dissertation.

The stress and temperature evolve according to the first and second equations in Eq. (2.31), expressed in rate form as

$$\begin{aligned} \dot{\boldsymbol{\tau}} &= \frac{\partial^2 u}{\partial \boldsymbol{\varepsilon}^{\mathrm{e}} \partial \boldsymbol{\varepsilon}^{\mathrm{e}}} \mathbin{:} \dot{\boldsymbol{\varepsilon}}^{\mathrm{e}} + \frac{\partial^2 u}{\partial \boldsymbol{\varepsilon}^{\mathrm{e}} \partial s}\dot{s} + \sum_{k=1}^{n} \frac{\partial^2 u}{\partial \boldsymbol{\varepsilon}^{\mathrm{e}} \partial q_k}\dot{q}_k \\ \rho_0 \dot{\theta} &= \frac{\partial^2 u}{\partial s^2}\dot{s} + \frac{\partial^2 u}{\partial s \partial \boldsymbol{\varepsilon}^{\mathrm{e}}} \mathbin{:} \dot{\boldsymbol{\varepsilon}}^{\mathrm{e}} + \sum_{k=1}^{n} \frac{\partial^2 u}{\partial s \partial q_k}\dot{q}_k \end{aligned} \tag{2.36}$$

Using the Maxwell relations in Eq. (2.24), these relationships can be expressed as

$$\begin{aligned} \dot{\boldsymbol{\tau}} &= \mathbb{C}_s \mathbin{:} \dot{\boldsymbol{\varepsilon}}^{\mathrm{e}} - \rho_0 \theta \boldsymbol{\Gamma} \dot{s} - \sum_{k=1}^{n} \frac{\partial \psi_k}{\partial \boldsymbol{\varepsilon}^{\mathrm{e}}}\dot{q}_k \\ \dot{\theta} &= \frac{\theta}{c_v}\dot{s} - \theta \boldsymbol{\Gamma} \mathbin{:} \dot{\boldsymbol{\varepsilon}}^{\mathrm{e}} - \frac{1}{\rho_0}\sum_{k=1}^{n} \frac{\partial \psi_k}{\partial s}\dot{q}_k \end{aligned} \tag{2.37}$$

2.5.3 Plastic Flow

For strain controlled loading, the solution to the plasticity problem begins by computing the "trial" stress, in which it is assumed that the entire strain increment is elastic. For adiabatic conditions, the trial stress rate is given by

$$\dot{\boldsymbol{\tau}}^{\text{trial}} = \mathbb{C}_s : \dot{\boldsymbol{\varepsilon}} \tag{2.38}$$

and the trial stress can be found by first order integration of Eq. (2.38)

$$\boldsymbol{\tau}_{\text{n+1}}^{\text{trial}} = \boldsymbol{\tau}_{\text{n}} + \dot{\boldsymbol{\tau}}_{\text{n+1}}^{\text{trial}} \Delta t \tag{2.39}$$

If $f(\boldsymbol{\tau}_{\text{n+1}}^{\text{trial}}, \xi) > 0$, plastic flow occurs and corrections to the trial state state are needed to satisfy the yield criterion $f(\boldsymbol{\tau}_{\text{n+1}}^{\text{trial}}, \xi) \leq 0$. Assuming an additive decomposition of the strain rate into elastic and plastic parts, the rates of stress and entropy in Eq. (2.37) for the plastic state are be given by

$$\begin{aligned} \dot{\boldsymbol{\tau}} &= \mathbb{C}_s : (\dot{\boldsymbol{\varepsilon}} - \dot{\boldsymbol{\varepsilon}}^{\text{p}}) - \rho_0 \theta \boldsymbol{\Gamma} \dot{s} - \sum_{k=1}^{n} \frac{\partial \psi_k}{\partial \boldsymbol{\varepsilon}^{\text{e}}} \dot{q}_k \\ \dot{\theta} &= \frac{\theta}{c_v} \dot{s} - \theta \boldsymbol{\Gamma} : (\dot{\boldsymbol{\varepsilon}} - \dot{\boldsymbol{\varepsilon}}^{\text{p}}) - \frac{1}{\rho_0} \sum_{k=1}^{n} \frac{\partial \psi_k}{\partial s} \dot{q}_k \end{aligned} \tag{2.40}$$

The rate of plastic strain can be conveniently expressed in terms of its magnitude and direction

$$\dot{\boldsymbol{\varepsilon}}^{\text{p}} = \dot{\lambda} \boldsymbol{m} \tag{2.41}$$

where $\dot{\lambda}$ is the magnitude of the rate of plastic deformation and $\boldsymbol{m}$ is its direction, given by the constitutive relation [12]

$$\boldsymbol{m} = \frac{\partial \varphi / \partial \boldsymbol{\tau}}{\| \partial \varphi / \partial \boldsymbol{\tau} \|} \tag{2.42}$$

where φ is the flow "potential". If $\varphi = f$ the flow rule is said to be associative and $\boldsymbol{m} = \boldsymbol{n}$, where $\boldsymbol{n}$ is the yield surface normal, defined as

$$\boldsymbol{n} = \frac{\partial f / \partial \boldsymbol{\tau}}{\| \partial f / \partial \boldsymbol{\tau} \|} \tag{2.43}$$

Assuming each internal state variable q_k changes only in response to plastic loading, they too can be expressed in terms of $\dot{\lambda}$ as

$$q_k = h_k \dot{\lambda} \tag{2.44}$$

where h_k is the modulus corresponding to each internal state variable. Substituting Eq. (2.41) and Eq. (2.44) into Eq. (2.40) gives the nonlinear coupled evolution of the stress and temperature

$$\begin{aligned} \dot{\boldsymbol{\tau}} &= \mathbb{C}_s : \left(\dot{\boldsymbol{\varepsilon}} - \dot{\lambda} \boldsymbol{m} \right) - \rho_0 \theta \boldsymbol{\Gamma} \dot{s} - \dot{\lambda} \sum_{k=1}^{n} \frac{\partial \psi_k}{\partial \boldsymbol{\varepsilon}^{\text{e}}} h_k \\ \dot{\theta} &= \frac{\theta}{c_v} \dot{s} - \theta \boldsymbol{\Gamma} : \left(\dot{\boldsymbol{\varepsilon}} - \dot{\lambda} \boldsymbol{m} \right) - \dot{\lambda} \sum_{k=1}^{n} \frac{\partial \psi_k}{\partial s} h_k \end{aligned} \tag{2.45}$$

Using the balance of energy in Eq. (2.32), the rate of stress and temperature (assuming adiabatic conditions with no heat sources) in Eq. (2.45) can be expressed as

$$\begin{aligned}\dot{\boldsymbol{\tau}} &= \dot{\boldsymbol{\tau}}^{\text{trial}} - \dot{\lambda}\left(\mathbb{C}_s \boldsymbol{:} \boldsymbol{m} + \boldsymbol{\Lambda}\right) \\ &= \dot{\boldsymbol{\tau}}^{\text{trial}} - \dot{\lambda}\boldsymbol{p} \qquad (2.46)\\ \dot{\theta} &= \dot{\theta}^{\text{trial}} - \dot{\lambda} P_\theta \qquad (2.47)\end{aligned}$$

where $\dot{\boldsymbol{\tau}}^{\text{trial}}$ is the "trial" stress rate found by presuming the entire strain increment is elastic, $\boldsymbol{p}$, the "return direction", is given by $\boldsymbol{p} = \mathbb{C}_s \boldsymbol{:} \boldsymbol{m} + \boldsymbol{\Lambda}$, and the elastic-plastic coupling tensor $\boldsymbol{\Lambda}$ and P_θ are given by

$$\boldsymbol{\Lambda} = (\boldsymbol{\tau} \boldsymbol{:} \boldsymbol{m})\boldsymbol{\Gamma} + \sum_{k=1}^{n} \left(\psi_k \boldsymbol{\Gamma} + \frac{\partial \psi_k}{\partial \boldsymbol{\varepsilon}^{\text{e}}} \right) h_k \qquad (2.48)$$

$$P_\theta = -\frac{1}{\rho_0 c_v} \boldsymbol{\tau} \boldsymbol{:} \boldsymbol{m} - \theta \boldsymbol{\Gamma} \boldsymbol{:} \boldsymbol{m} - \frac{1}{\rho_0} \sum_{k=1}^{n} \left(\frac{\psi_k}{c_v} - \frac{\partial \psi_k}{\partial s} \right) h_k \qquad (2.49)$$

Specific forms of the h_k depend on the evolution equations for q_k.

The value of $\dot{\lambda}$ is found by requiring that, after the onset of yield, the stress remain on the yield surface. This requirement, known as the consistency condition, is represented mathematically by

$$\dot{f} = \frac{\partial f}{\partial \boldsymbol{\tau}} \boldsymbol{:} \dot{\boldsymbol{\tau}} + \frac{\partial f}{\partial \theta} \dot{\theta} + \frac{\partial f}{\partial q_k} \dot{q}_k = 0 \qquad (2.50)$$

dividing by $\|\partial f / \partial \boldsymbol{\tau}\|$ to normalize, gives

$$\boldsymbol{n} \boldsymbol{:} \dot{\boldsymbol{\tau}} = G\dot{\lambda} + \Theta\dot{\theta} \qquad (2.51)$$

where G, and Θ are given by

$$G = -\frac{\partial f / \partial q_k}{\|\partial f / \partial \boldsymbol{\tau}\|} h_k, \quad \Theta = -\frac{\partial f / \partial \theta}{\|\partial f / \partial \boldsymbol{\tau}\|} \qquad (2.52)$$

Substituting Eq. (2.49) and Eq. (2.48) into Eq. (2.51) and solving for $\dot{\lambda}$ gives

$$\dot{\lambda} = \frac{\left(\boldsymbol{n} \boldsymbol{:} \mathbb{C}_s + \Theta\theta\boldsymbol{\Gamma}\right) \boldsymbol{:} \dot{\boldsymbol{\varepsilon}}}{H + \boldsymbol{n} \boldsymbol{:} \mathbb{C}_s \boldsymbol{:} \boldsymbol{m} + \boldsymbol{n} \boldsymbol{:} \boldsymbol{\Lambda}} \qquad (2.53)$$

where H is the ensemble hardening modulus given by

$$H = G - \Theta P_\theta \qquad (2.54)$$

It can be shown that first order integration of Eq. (2.46) leads to an updated stress of the following form [12], whether or not the strain increment was partially or fully plastic

$$\boldsymbol{\tau}^{\text{new}} = \boldsymbol{\tau}^{\text{trial}} - \Lambda \boldsymbol{p} \qquad (2.55)$$

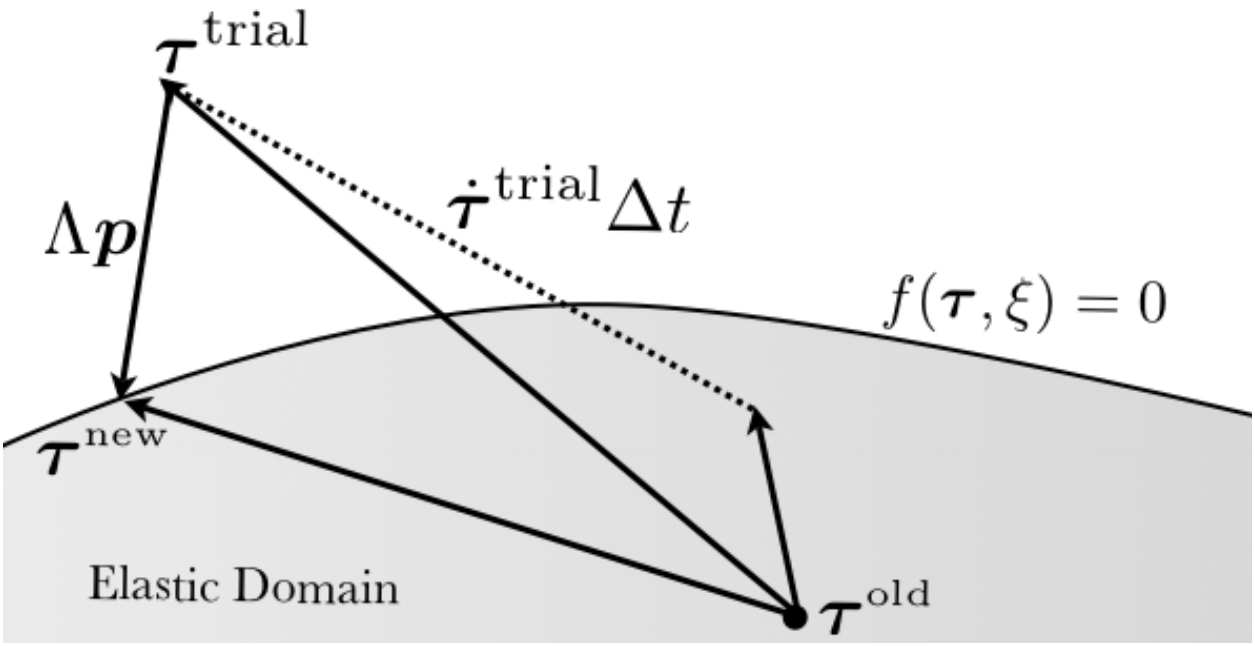

Figure 2.1. Oblique return projection of the trial stress state on to the yield function isosurface.

where the scalar Λ is determined by requiring that $f(\boldsymbol{\tau}^{\text{trial}} - \Lambda \boldsymbol{p}) = 0$ and can be found by a variety of numerical methods.

Equation (2.55) admits a convenient physical interpretation: the updated stress $\boldsymbol{\tau}^{\text{new}}$ is the oblique projection of $\boldsymbol{\tau}^{\text{trial}}$ on to the yield surface defined by $f(\boldsymbol{\tau}, \xi) = 0$, $\boldsymbol{p}$ is the direction of the projection, and Λ is its magnitude, as depicted in Figure 2.1.

Thus completes the system of equations for the stress and temperature evolution in a thermoplastic material. For further details consult [12]. Discussion of how to solve the resulting system of equations will be postponed until later in this document.

2.5.4 Temperature Evolution Due to Plastic Dissipation – Comparison with Common Form Found in Literature

For the case of adiabatic loading of a thermoplastic material, common in applications which involve high rates of deformation, and in the absence of any heat sources, it was shown that the temperature evolved according to

$$\dot{\theta} = -\theta \boldsymbol{\Gamma} : \dot{\boldsymbol{\varepsilon}}^{\text{e}} + \frac{1}{\rho_0 c_v} \boldsymbol{\tau} : \dot{\boldsymbol{\varepsilon}}^{\text{p}} + \frac{1}{\rho_0} \sum_{k=0}^{n} \left(\frac{1}{c_v} \psi_k - \frac{\partial \psi_k}{\partial s} \right) \dot{q}_k \tag{2.56}$$

In the literature, the temperature evolution in a thermoplastic material is often expressed as

$$\dot{\theta} = \frac{\chi}{\rho_0 c_v} \boldsymbol{\tau} : \dot{\boldsymbol{\varepsilon}}^{\mathrm{p}} \tag{2.57}$$

where χ, known as the Taylor-Quinney coefficient and is commonly assigned a constant value between 0.7 and 1.0, a reflection of the experimental evidence that not all plastic work is converted to heat [13]. Writing Eq. (2.56) in the above form we get the following for the Taylor-Quinney coefficient

$$\chi = 1 - \frac{1}{\boldsymbol{\tau} : \dot{\boldsymbol{\varepsilon}}^{\mathrm{p}}} \left[\theta \boldsymbol{\Gamma} : \dot{\boldsymbol{\varepsilon}}^{\mathrm{e}} + \frac{1}{\rho_0} \sum_{k=0}^{n} \left(\frac{\partial \psi_k}{\partial s} - \frac{1}{c_v} \psi_k \right) \dot{q_k} \right] \tag{2.58}$$

Clearly, χ evolves with both θ and q_k and, thus, should not be assumed to be constant. Doing so will undoubtedly lead to errors in model predictions which can lead to the assignment of erroneous values of model parameters to match experimental data. Rosakis et al.[11] derived a similar expression for χ and developed a series of experiments to measure χ indirectly.

Note that, depending on the specific form of the functions ψ_k and $\dot{q_k}$, Eq. (2.56) has the desired quality that only a portion of the plastic work is converted to heat without resorting to introducing empirical parameters such as χ.

2.5.5 Viscoplasticity

For a rate dependent viscoplastic material, the stress state is allowed to move beyond the yield surface, but returns to the surface as the rate of plastic deformation decreases. This apparent increase in strength with increasing strain rate is termed the "over-stress". In the Duvaut-Lions over-stress formulation [14], the dynamic transient stress state is attracted to the quasi-static stress state through the materials relaxation time, τ. Further details of the overstress model employed in Thermo-Kayenta can be found in the Kayenta user's manual [2].

Chapter 3

Constitutive Models for Thermoplastic Materials

In the previous chapter, an overview of thermomechanics and the governing equations of classical plasticity was made. In this chapter, Sandia National Laboratory's Kayenta plasticity model, Johnson-Cook plasticity, and the Mie-Grüneisen equation of state will be reviewed with emphasis on giving the background necessary to understand the recent thermal development in Kayenta. For more detailed explanations of these three models please refer to the cited references.

3.1 Kayenta

In Kayenta [1], the yield criterion is given by

$$\sqrt{J_2} = \frac{f_f(I_1) f_c(I_1, \kappa)}{L(\theta)} \tag{3.1}$$

and the yield function by

$$f(\boldsymbol{\sigma}, \boldsymbol{\alpha}, \kappa) = J_2^{\boldsymbol{\xi}} L\left(\theta^{\boldsymbol{\xi}}\right) - f_f(I_1)^2 f_c(I_1, \kappa) \tag{3.2}$$

where F_f and Γ are used to describe the elastic limit caused by the presence of microcracks, F_c accounts for strength reduction due to porosity, and κ is an internal state variable whose value controls the hydrostatic elastic limit. $J_2^{\boldsymbol{\xi}}$ and $\theta^{\boldsymbol{\xi}}$ are the second mechanics invariant and lode angle associated with the shifted stress tensor $\boldsymbol{\xi} = \boldsymbol{\sigma} - \boldsymbol{\alpha}$, where $\boldsymbol{\alpha}$ is the backstress associated with kinematic hardening.

If kinematic hardening is enabled, the backstress tensor evolves proportional to the deviatoric part of the plastic strain rate:

$$\dot{\boldsymbol{\alpha}} = H g(\boldsymbol{\alpha}) \dot{\boldsymbol{\gamma}}^{\mathrm{p}} \tag{3.3}$$

where

$$\dot{\boldsymbol{\gamma}}^{\mathrm{p}} = \operatorname{dev} \dot{\boldsymbol{\varepsilon}}^{\mathrm{p}} \tag{3.4}$$

and H is a material constant. Since the backstress evolves with the plastic strain, it is regarded as an internal state variable and can be written in the form shown in Eq. (2.44):

$$\dot{\boldsymbol{\alpha}} = \boldsymbol{H}_\alpha \dot{\lambda} \tag{3.5}$$

where $\boldsymbol{H}_\alpha$ is the kinematic hardening tensor. Comparing Eq. (3.5) to Eq. (3.3) leads to

$$\boldsymbol{H}_\alpha = H g\left(\boldsymbol{\alpha}\right) \operatorname{dev} \frac{\partial \varphi}{\partial \boldsymbol{\xi}} \tag{3.6}$$

In the above equations, $g\left(\right)$ is a scalar valued decay function which limits the kinematic hardening so that the stress cannot exceed the shear limit surface, defined as

$$g\left(\boldsymbol{\alpha}\right) = 1 - \frac{\sqrt{J_2^{\boldsymbol{\xi}}}}{N} \tag{3.7}$$

3.2 Johnson-Cook Plasticity

In classical Johnson-Cook plasticity [4, 15], the flow stress is given by the empirical relation

$$\sigma_{\mathrm{y}} = \left[A + B\gamma_{eq}^{n}\right]\left[1 + C\ln\dot{\gamma}_{\mathrm{eq}}^{*}\right]\left[1 - (\theta^{*})^{m}\right] \tag{3.8}$$

where γ_{eq} is the equivalent plastic strain, $\dot{\gamma}_{\mathrm{eq}}^{*}$ is a normalized plastic strain-rate, $A, B, C, n,$ and m are material constants, and θ^{*} is the homologous temperature. The normalized strain-rate and temperature are defined as

$$\dot{\gamma}_{\mathrm{eq}}^{*} = \frac{\dot{\gamma}_{\mathrm{eq}}}{\dot{\gamma}_0}, \quad \theta^{*} = \frac{\theta - \theta_0}{\theta_{\mathrm{m}} - \theta_0} \tag{3.9}$$

where $\dot{\gamma}_0$ is a user defined plastic strain-rate, θ_0 is a reference temperature, and θ_{m} is a reference melting temperature.

In addition to publishing detailed procedures for choosing values for the material constants $A,\ B,\ C,\ n,\ m$ and $\dot{\gamma}_0$, Johnson and Cook published large tables of calibration data for a wide range of materials. This, combined with the models simplicity, has led to the Johnson-Cook flow rule to becoming one of the most widely used thermoplasticity models today. It is also available as a built in material definition in nearly every commercial finite element code, furthering its use nearly 25 years after its introduction. Regular use notwithstanding, the Johnson-Cook flow stress model is, at its core, a hardening Von-Mises type flow rule with strain rate hardening and temperature dependence included through the multipliers $1 + C\ln\dot{\gamma}_{\mathrm{eq}}^{*}$ and $1 - (\theta^{*})^{m}$. It is well established that the overly-simplistic Von-Mises flow rule is insufficient for modeling complex phenomena and materials [3, 16]. Wright [10] argues that the temperature term should be considered unsatisfactory because it either vanishes at θ_0 $(m > 0)$ or is infinite there $(m < 0)$; and that for the common case that $m = 1$, the initial thermal softening is determined solely by the magnitude of the melt temperature θ_{m}. All

three of these cases are physically unlikely, particularly in the case where the functional form of the temperature dependence of the yield strength changes due to phase changes within the material.

Furthermore, the Johnson-Cook flow stress model is wholly empirical and, thus, its performance is highly dependent on its calibration data. In other words, simulations performed outside of the class of problems used for calibrating the model should be considered highly suspect. This leaves a large hole in the models usefulness as calibration data typically only exists for few[1] of the infinitely many loading paths.

For a comparison of the Johnson-Cook model with other thermoplasticity models as implemented in the University of Utah's Uintah MPM code see [17].

3.3 Mie-Gruneisen Equation of State

The outline of the Mie-Güneisenequation of state closely follows the treatment given by Drumheller [8] which can be consulted for further details. Strictly speaking, the Mie-Güneisenequation of state is not a thermoplastic model, but an equation of state relating energy, density, pressure, and temperature. However, the Mie-Güneisenequation of state is an important component in many thermoplasticity models as it is used to compute the bulk response of the thermoplastic material undergoing large compressive deformation.

In the Mie-Güneisensolid, it is assumed that the internal energy can be decomposed additively into "cold" and "thermal" parts

$$u = u_c(\rho) + u_\theta(\rho, s) \tag{3.10}$$

It is further assumed that the thermal energy can be decomposed multiplicatively in its arguments so that

$$\ln \frac{u - u_c}{u_0} = \int_{\rho_0}^{\rho} \frac{\gamma(\rho')}{\rho'}\, d\rho' + \int_{s_0}^{s} \frac{1}{c_v(s')}\, ds' \tag{3.11}$$

where $\gamma(\rho)$ and $c(s)$ are functional forms of the Grüneissenparameter and the specific heat. Equation Eq. (3.11) now describes the equilibrium energy of the Mie-Güneisensolid. The partial derivative of Eq. (3.11) with respect to J gives

$$\left(\frac{1}{u - u_c}\right)\left(\left(\frac{\partial u}{\partial J}\right)_s - \frac{du_c}{dJ}\right) = -\frac{\gamma}{J} \tag{3.12}$$

Simplifying Eq. (3.12),

$$\frac{1}{\rho_0}\left(\frac{\partial u}{\partial V}\right)_s = \frac{1}{\rho_0}\frac{du_c}{dV} - \frac{1}{\rho_0} c_v \theta \gamma \rho \tag{3.13}$$

[1]Calibration data is typically only available from uniaxial strain, uniaxial stress, and dynamic torsion tests.

where V is the specific volume and we have used $u - u_c = u_\theta = c_v\theta$.[2] Multiplying Eq. (3.13) by ρ_0, the equilibrium pressure in a Mie-Güneisensolid is defined as

$$p = p_c + p_\theta \tag{3.14}$$

where

$$\begin{aligned} p &= -\frac{\partial u}{\partial V} \\ p_c &= -\frac{\partial u_c}{\partial V} \\ p_\theta &= \rho\gamma c_v\theta \end{aligned} \tag{3.15}$$

Using shock Hugoniot data as a reference instead of the cold state, the pressure in Mie-Güneisensolid is given by

$$\begin{aligned} p &= p_H + \gamma_0\rho_0\left(u - u_H\right) \\ \theta &= \theta_H + \frac{1}{c_v}\left(u - u_H\right) \end{aligned} \tag{3.16}$$

where p_H, u_H, and θ_H are the Hugoniot pressure, energy, and temperature, respectively which are determined from the Hugoniot. The Hugoniot is given by

$$\boldsymbol{v}_s = c_s + s_1\boldsymbol{v}_p + \frac{s_2}{c_s}\boldsymbol{v}_p^2 \tag{3.17}$$

where c_s, s_1, and s_2 are constants determined by experiment.

A detailed description of the Mie-Güneisensolid and derivations of Eq. (3.16) and Eq. (3.17) can be found in Chapter 4 of [8].

[2]The relation $u_\theta = c_v\theta$ can be seen by taking the partial derivative of Eq. (3.11) with respect to s

Chapter 4

Incorporating Thermal Effects in Kayenta: Initial Development

In the previous chapters, overviews of thermomechanics of solids, Kayenta, and Johnson-Cook constitutive models were made. As previously noted, the equation of state in previous releases of Kayenta was purely mechanical and could not adequately predict material response to deformation when thermal effects were non-negligible, as in metals. It also goes without saying, that these previous releases of Kayenta did not satisfy the balance and dissipation laws given in Chapter 2. Nevertheless, Kayenta's extensive feature set and ability to reduce to a number of classical plasticity models make it an attractive base model to which thermal effects can be included.

In this chapter, an overview of the implementation of thermomechanics in Kayenta will be made. To distinguish this version of Kayenta from previous versions which had no thermodynamic considerations, it will be referred to as "Thermo-Kayenta". In the sections that follow, descriptions of how thermomechanics is implemented in Thermo-Kayenta will be given.

4.1 Thermoelasticity

Because Thermo-Kayenta presumes that the material, its stiffness tensor $\mathbb{C}$, and Grüneissentensor $\mathbf{\Gamma}$ are isotropic, the stress rate in Eq. (2.40) is decomposed additively into isotropic and deviatoric responses

$$\dot{\boldsymbol{\tau}} = -\kappa^* \dot{\varepsilon}_{\mathrm{v}} \boldsymbol{I} + 2\mu^* \dot{\boldsymbol{\gamma}} \tag{4.1}$$

where κ^* and μ^* are the effective tangent bulk and shear moduli, respectively and $\dot{\boldsymbol{\gamma}}$ is the strain deviator defined in the usual way as

$$\dot{\boldsymbol{\gamma}} = \dot{\boldsymbol{\varepsilon}} - \frac{1}{3}\dot{\varepsilon}_{\mathrm{v}} \boldsymbol{I} \tag{4.2}$$

The temperature response, in general, is given by

$$\dot{\theta} = \dot{\theta}(\kappa, \dot{\boldsymbol{\varepsilon}}) \tag{4.3}$$

The specific forms of $\dot{\theta}(\kappa, \dot{\boldsymbol{\varepsilon}})$ and the effective bulk and shear moduli are determined by the value of the user input IEOSID. If IEOSID=0 (default), then the effective moduli are computed by

$$\begin{aligned} \kappa^* &= \kappa(I_1)\left(1 - \frac{\rho^2}{\rho_0}\theta c_v \gamma^2\right) \\ \mu^* &= \mu(J_2) \end{aligned} \tag{4.4}$$

and

$$\dot{\theta}(\kappa, \dot{\boldsymbol{\varepsilon}}) = -\frac{\rho}{\rho_0}\theta\gamma\dot{\varepsilon}_{\mathrm{v}} \tag{4.5}$$

where $\kappa(I_1)$ and $\mu(J_2)$ are the standard non-linear elastic tangent bulk and shear moduli functions already in Kayenta. If $\gamma = 0$, Eq. (4.4) reduces to the same bulk modulus functions used in previous releases of Kayenta.

Note that the effective bulk modulus in Eq. (4.4) is the standard *isentropic* bulk modulus and requires that $\kappa(I_1)$ be the *isothermal* bulk modulus. However, as explained in the Kayenta User's Manual, the nonlinear function $\kappa(I_1)$ returns a value which is an interpolation between the isothermal and isentropic bulk moduli. Thus, if IEOSID=0, it is recommended that either: 1) γ be set to zero if $B1 - B2$ are non-zero, or 2) $B1 - B2$ be set to zero if γ is non-zero.

If IEOSID=0 and $B1 - B2$ are set equal to zero, Thermo-Kayenta reduces to thermoelasticity as explained in Chapter 2.

If IEOSID=1, the effective tangent elastic moduli are computed from an equation of state specified in the subroutine `EOSMODULI`. Currently, Thermo-Kayenta uses SNL's Kerley Mie-Grüneisen equation of state which takes as input the current density and energy and returns the updated pressure, temperature, and soundspeed. κ^* and μ^* are then computed by

$$\begin{aligned} \kappa^* &= \rho {c_{\mathrm{B}}}^2 \\ \mu^* &= 3\kappa^* \frac{1 - 2\nu}{2(1 + \nu)} \end{aligned} \tag{4.6}$$

where c_{B} is the bulk speed of sound in the material and ν is Poisson's ratio and is assumed to be constant.

To date, every installation of Kayenta has approximated the strain rate by the symmetric part of the velocity gradient. Thus, u is updated internally in Thermo-Kayenta by

$$u = \frac{1}{\rho_0}\boldsymbol{\tau}\!:\!\boldsymbol{d} \tag{4.7}$$

4.2 Thermoelastic Limit

If the trial elastic stress found in the previous section lies outside of the yield surface given by Eq. (3.2), the tentatively presumed elastic loading is invalidated and the solution to the

equations governing thermoplastic loading must be solved. For the case of a thermoplastic material, the yield criterion in Eq. (3.1) is modified to allow for thermal softening in a way similar to Johnson-Cook plasticity by including a non-dimensional multiplier in the yield function, as follows:

$$\sqrt{J_2\boldsymbol{\xi}} = \frac{f_f(I_1)f_c(I_1,\kappa)}{L\left(\theta^{\boldsymbol{\xi}}\right)}\left(1-(\theta^*)^m\right) \tag{4.8}$$

For the case that $f_c = 1$ and $\Gamma = 1$, Eq. (4.8) reduces to

$$\sqrt{J_2\boldsymbol{\xi}} = \left(a_1 - a_3\mathrm{e}^{-a_2 I_1} + a_4 I_1\right)\left(1-(\theta^*)^m\right) \tag{4.9}$$

where m is taken to be the same user specified constant as in Johnson-Cook plasticity. θ^* is defined in the same way as in the Johnson-Cook plasticity model:

$$\theta^* = \frac{\theta-\theta_0}{\theta_\mathrm{m}-\theta_0} \tag{4.10}$$

4.3 Evolution Equations

4.3.1 Kinematic Hardening Backstress Tensor

If kinematic hardening is enabled, the evolution of the backstress in a thermoplastic material governed by

$$\dot{\boldsymbol{\alpha}} = \dot{\lambda}\boldsymbol{H}^\star_{\boldsymbol{\alpha}} \tag{4.11}$$

where $\boldsymbol{H}^\star_{\boldsymbol{\alpha}}$ is given by

$$\boldsymbol{H}^\star_{\boldsymbol{\alpha}} = Hg\left(\boldsymbol{\alpha}\right)^* \operatorname{dev}\frac{\partial\varphi}{\partial\boldsymbol{\xi}} \tag{4.12}$$

and

$$g\left(\boldsymbol{\alpha}\right)^* = g\left(\boldsymbol{\alpha}\right)\left(1-(\theta^*)^m\right) \tag{4.13}$$

4.3.2 Plastic Temperature Evolution

Currently, all plastic work is converted to heat, thus the temperature evolves according to

$$\dot{\theta} = \dot{\theta}^{\mathrm{trial}} + \frac{1}{\rho_0}\left[\left(\rho_0\theta\gamma + \frac{1}{c_v}I_1\right)\dot{\varepsilon}^{\mathrm{p}}_{\mathrm{v}} + \frac{1}{c_v}\boldsymbol{\mathcal{S}}\boldsymbol{:}\dot{\boldsymbol{\gamma}}^{\mathrm{p}}\right] \tag{4.14}$$

Chapter 5

Incorporating Thermal Effects in Kayenta: Solution Scheme

In the previous chapter, the thermo-mechanical equations solved by Thermo-Kayenta were described. In this chapter, we describe from a more global perspective how thermodynamics fits into the Kayenta framework. In addition, installation instructions as well as a description of additional thermal arguments required from the host code will be described. The chapter finishes with Thermo-Kayenta's solution algorithm.

5.1 Role of Thermodynamics in Kayenta

Thermo-Kayenta distinguishes itself from most thermoplasticity models, by requiring no explicit input from the host code regarding the varying thermal state, as it is computed and tracked internally by the model. This is made possible because of the initial assumption of adiabatic conditions common in shock loading, thus, Thermo-Kayenta may not be appropriate for slow rate quasistatic simulations.

The advantages of tracking thermal variables internally, as opposed to receiving them from the host code are

- Consistency with the theory of thermomechanics.
- A consistently updated thermal state is available during subcycle loops.
- Thermo-Kayenta only requires from the host code (besides storage of internal state variables) the strain rate at the beginning of the step.
- Thermo-Kayenta can be installed in *any* host code which is capable of calling external material models written in FORTRAN.

It might be argued that the temperature and energy at the beginning of each time step should be supplied by the host code after solving the heat equation. We counter that argument by reminding the reader that the derivation and implementation of thermodynamics in Thermo-Kayenta were based on the assumption of *adiabatic* loading, common in shock physics. Thus,

it would make little sense for the host code to conduct the adiabatic temperature returned by Thermo-Kayenta. Of course, model installers are free to replace the temperature and energy in the state variable array with the updated temperature and energy, as calculated by the host code, at the beginning of each timestep, though this is not recommended by the Thermo-Kayenta developers.

5.2 Installation of Thermo-Kayenta

For MIG [18] compliant host codes in which Kayenta is already installed, installing Thermo-Kayenta requires only replacing the previous version of the Kayenta source code with the new Thermo-Kayenta source code. Of course, new input sets will also be required which reflect the additional thermal properties needed by the model. The ease of installation is possible because all time varying thermal variables are tracked by Thermo-Kayenta internally in the internal state variable array. These variables, as well as the additional files and subroutines Thermo-Kayenta adds to Kayenta, are explained in the remainder of this chapter.

Thermo-Kayenta has also been successfully installed the non-MIG compliant host codes Abaqus and LS-Dyna. Contact the model developers for more information on installing Thermo-Kayenta in these, and other, non-MIG compliant codes.

5.3 Thermo-Kayenta Files, Subroutines, and Functions

Thermo-Kayenta adds two FORTRAN77 files, Kayenta_therm.F and Kayenta_eos.F, to the existing Kayenta framework which contain the following *private* subroutines and functions:

Kayenta_therm.F:

`EOSCHK` Subroutine. Companion subroutine to `GEOCHK`. Checks validity of user inputs for the equation of state.

`THERMO_INIT` Subroutine. Initializes thermal state variables.

`KAYENTA_MODULI` Subroutine. Determines the non-linear elastic properties using either the standard Kayenta nonlinear elastic property functions or an equation of state, depending on the value of the user input IEOSID.

`EOSMODULI` Subroutine. Evaluates the equation of state. Currently, `EOSMODULI`, calls the Kerley Mie-Güneisen equation of state. At the discretion of the user, other *user* defined equations of state can be called from within this subroutine. Doing so will require modifying this subroutine to call the desired equation of state. Undoubtedly, the

THERMO_INIT and EOSCHK subroutines would also have to be modified. The Thermo-Kayenta developers do not currently support changing the equation of state from the supplied Kerley Mie-Güneisen equation of state.

TMULT Function. Evaluates $(1-(\theta^*)^m)$ in Eq. (4.10).

ENINC Function. Computes increment in internal energy $\Delta u = \frac{1}{\rho}\boldsymbol{\tau}\!:\!\Delta\boldsymbol{\varepsilon}$.

Kayenta_eos.F:

KEOSMGI Subroutine. Data check routine for Mie-Güneisenequation of state.

KEOSMGJ Subroutine. Computes temperature fit for Mie-Güneisenequation of state.

KEOSMGP Subroutine. Polynomial fit to energy function in the Mie-Güneisenequation of state.

KEOSMGY Subroutine. Integrates temperature function for Mie-Güneisenequation of state

KEOSMGR Subroutine. Pressure and energy as functions of density and temperature using Mie-Güneisenequation of state.

KEOSMGV Subroutine. Pressure and temperature as functions of density and energy using Mie-Güneisenequation of state.

5.4 Thermo-Kayenta I/O

Thermo-Kayenta *does not* add any additional calling arguments to Kayenta. However, some of the arrays passed to and from Thermo-Kayenta contain additional information. The following list, adapted from the Kayenta user manual, describes variables passed between the host code and Thermo-Kayenta's driver routine (Kayenta_calc). The variables in green are those modified from previous non-thermal releases of Kayenta and will be described in more detail in the following sections.

Input

NBLK The number of cells or finite elements to be processed. Parallel codes send only one cell at a time (NBLK=1).

NINSV The number of internal state variables for Kayenta.

DT The time step

PROP The user-input array, filled with real numbers. The additional arguments required by Thermo-Kayenta are described in the following sections and are also summarized within the source code prolog itself.

SIG The unrotated Cauchy stress tensor at time n. The six independent components of the stress must be passed in the ordering $\{\tau_{11}, \tau_{22}\ \tau_{33}, \tau_{12}, \tau_{23}$, and $\tau_{31}\}$. Within the FORTRAN, this array is dimensioned "SIG(6, NBLK)" so that the stress components for any given finite element are in six contiguous memory locations.

D The unrotated strain rate tensor, preferably evaluated at time n+1/2 because Kayenta treats the strain rate tensor as constant over the entire interval. Most codes approximate the strain rate tensor as the unrotated symmetric part of the velocity gradient. Component ordering and contiguous storage are the same as for stress.

SV The internal state variable array. The additional arguments required by Thermo-Kayenta are described in the following sections.

Output

SIG The unrotated stress tensor at time $n + 1$. The component ordering is the same as described above.

SV The internal state variable array (updated to time $n + 1$)

USM Uniaxial strain (constrained) elastic modulus equal to $H = \kappa + 4/3\mu$. The host code may use the USM output to compute an upper bound on the wave speed ($\sqrt{H/\rho}$, where ρ is mass density) when setting the timestep.

5.4.1 Thermal Property Array

The Thermo-Kayenta property array includes the following variables which must be specified by the user in addition to the regular Kayenta variables:

Thermal Properties Needed by the Strength Model and Equation of State

IEOSID – ID for equation of state type

TMPRXP – Temperature exponent, m

RHOO – Initial density

TMPRO – Initial temperature

CV – Heat capacity

GRPAR – Gruneisen parameter

Thermal Properties Needed Only by the Kerley Mie-GüneisenEquation of State

`SNDSP0` – Initial sound speed

`S1MG` – Linear coefficient in Hugoniot fit

`S2MG` – Quadratic coefficient in Hugoniot fit

`VI4MG` – Melt temperature

5.4.2 Thermal State Variable Array

It is in the state variable array that Thermo-Kayenta tracks the changing thermal state. The Thermo-Kayenta state variable array contains the following arguments in addition to the usual Kayenta array:

`TMPR` – Absolute temperature

`SNDSP` – Soundspeed

`RHO` – Mass density

`ENRGY` – Internal energy

5.5 Thermo-Kayenta Algorithm

The following algorithm is copied from the Kayenta User's Manual with modifications for Thermo-Kayenta highlighted in blue. References to equations of the form Eq. (x.xx) refer to equations in the Kayenta User's Manual that do not appear in this report.

Rate independent (inviscid) part of the viscoplasticity equations.

step 1. To guard against unpredictable host-code advection errors (or similar corruption of the updated state from the last time step), apply a return algorithm to ensure the initial stress is on or inside the yield surface.

step 2. Compute the nonlinear elastic tangent moduli using either the standard non-linear functions or Mie-Güneisenequation of state appropriate to the stress at time n.

step 3. Apply Hooke's law in rate form to obtain the thermoelastic stress and temperature rates at time n.

step 4. Integrate the thermoelastic stress and temperature rates using first-order differencing to obtain an estimate for the trial thermoelastic stress and temperature at the end of the step.

step 5. Evaluate the yield function at the trial thermoelastic stress and temperature. If the yield function evaluates to a negative number, the trial thermoelastic stress and temperature is accepted as the final updated stress and temperature, and the inviscid algorithm returns (i.e., go to STEP 16). Otherwise, continue.

step 6. To reach this step, the trial thermoelastic stress state was found to lie outside the yield surface. At this point, the time step is divided into an internally determined number of subcycles. All subsequent steps described below this point apply to the smaller time steps associated with subcycles.

step 7. Evaluate the gradients of the yield function for eventual use in Eq. (2.53).

step 8. Evaluate the flow potential gradients for eventual use in Eq. (2.53).

step 9. Evaluate the isotropic hardening coefficient in Eq. (4.73).

step 10. Evaluate the function in Eq. (4.12).

step 11. Apply Eq. (2.53) to obtain the consistency parameter.

step 12. Use forward differencing (within the subcycle) to integrate Eq. (4.73) and Eq. (4.12), thereby updating the internal state variables κ and α_{ij}.

step 13. The above steps will have directly integrated the governing equations through the end of the subcycle, so the updated stress will be in principle already on the yield surface. However, to guard against slight round-off and integration errors by applying an iterative return correction to place the stress exactly on the yield surface.

step 14. Increment the subcycle counter, and save the partially updated inviscid internal state variables.

step 15. If subcycles remain to be evaluated, go to STEP 7. Otherwise, continue to STEP 16.

Viscous part of the viscoplasticity equations.

step 16. The previous set of steps govern computation of the equilibrium state. Now apply Eq. (6.22) to compute the characteristic material response time.

step 17. Using the trial elastic stress corresponding to an update to the end of the time step, apply Eq. (6.10) to compute the dynamic stress. Apply Eq. (6.15) to similarly compute the dynamic values of internal state variables to account for rate sensitivity.

step 18. Save the values of the internal state variables into the state variable array.

step 19. STOP.

Chapter 6

Incorporating Thermal Effects in Kayenta: Verification of Results

We now review the results of simulations using Thermo-Kayenta and verify those results against identical simulations run using the Johnson-Cook plasticity model. Two types of verification tests were run: single element simulations using uniaxial, isotropic, and isochoric displacement controlled strain paths and a multi-element Taylor impact simulation.

All single element Johnson-Cook simulations were performed by Joseph Bishop on SNL's ALEGRA using identical Mie-Grüneisen equation of state subroutines while the single element Thermo-Kayenta simulations were performed in Prof. Rebecca Brannon's stand alone material driver, MED. Both the Johnson-Cook and Thermo-Kayenta Taylor impact simulations were performed in LS-Dyna.

In the following simulations, the following material properties were used in the models indicated:

A	B	C	m	n	θ_0	θ_m
90 MPa	292 MPa	0.025	1.09	0.31	298 K	1356 K

Table 6.1. Material properties used in the Johnson-Cook flow model

κ	μ	A_1	R	H	T_1
137 GPa	53.0 GPa	112.5 MPa	22.5 MPa	750 Gpa	

Table 6.2. Material properties used in Thermo-Kayenta

ρ_0	c	s_1	γ_0	c_v
8960.0 Kg/m^3	m/s	1.5	1.99	383.0 J·Kg/K

Table 6.3. Material properties used in the Mie-Güneisen equation of state

6.1 Case Study 1: Isotropic Deformation

Since Thermo-Kayenta, as does SNL's installation of Johnson-Cook plasticity in ALEGRA, presumes plastic incompressibility, comparison of isotropic deformation is used to verify calculations and installation of the equation of state in Thermo-Kayenta. For each of the following comparisons, the following prescribed volumetric strain path was used:

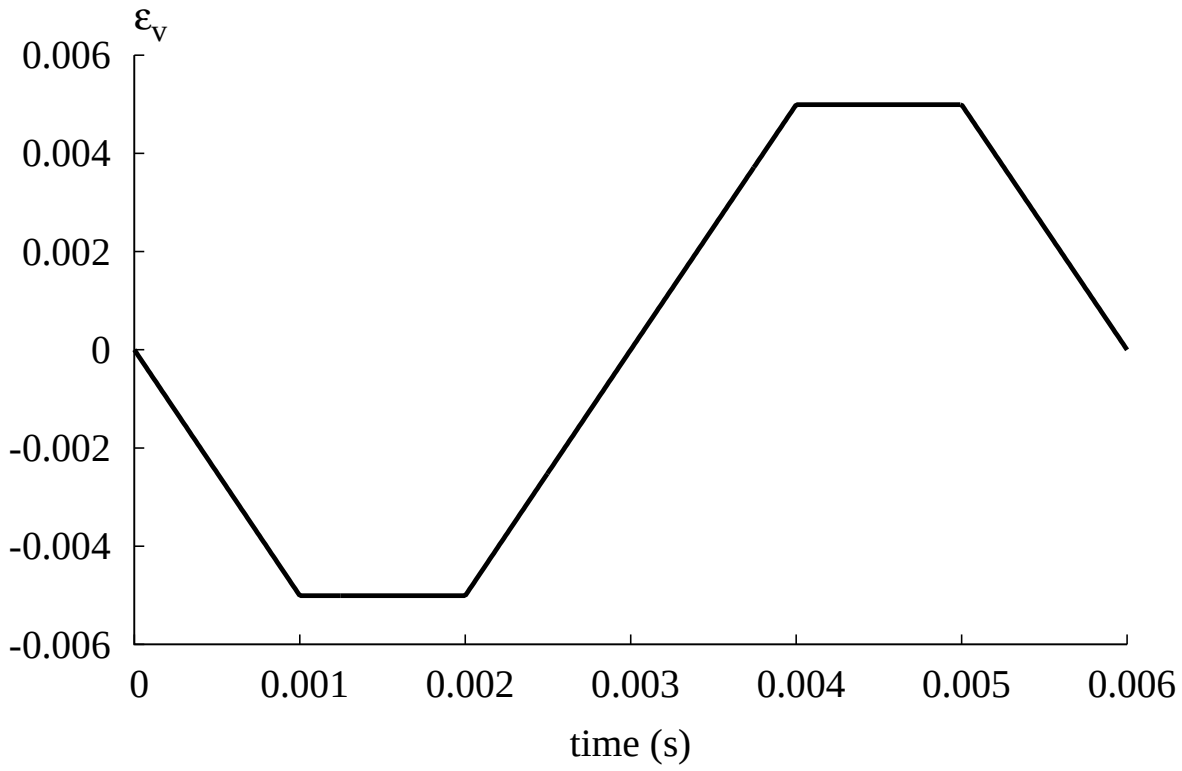

Figure 6.1. Prescribed isotropic strain path

6.1.1 Isotropic deformation - comparison of material response

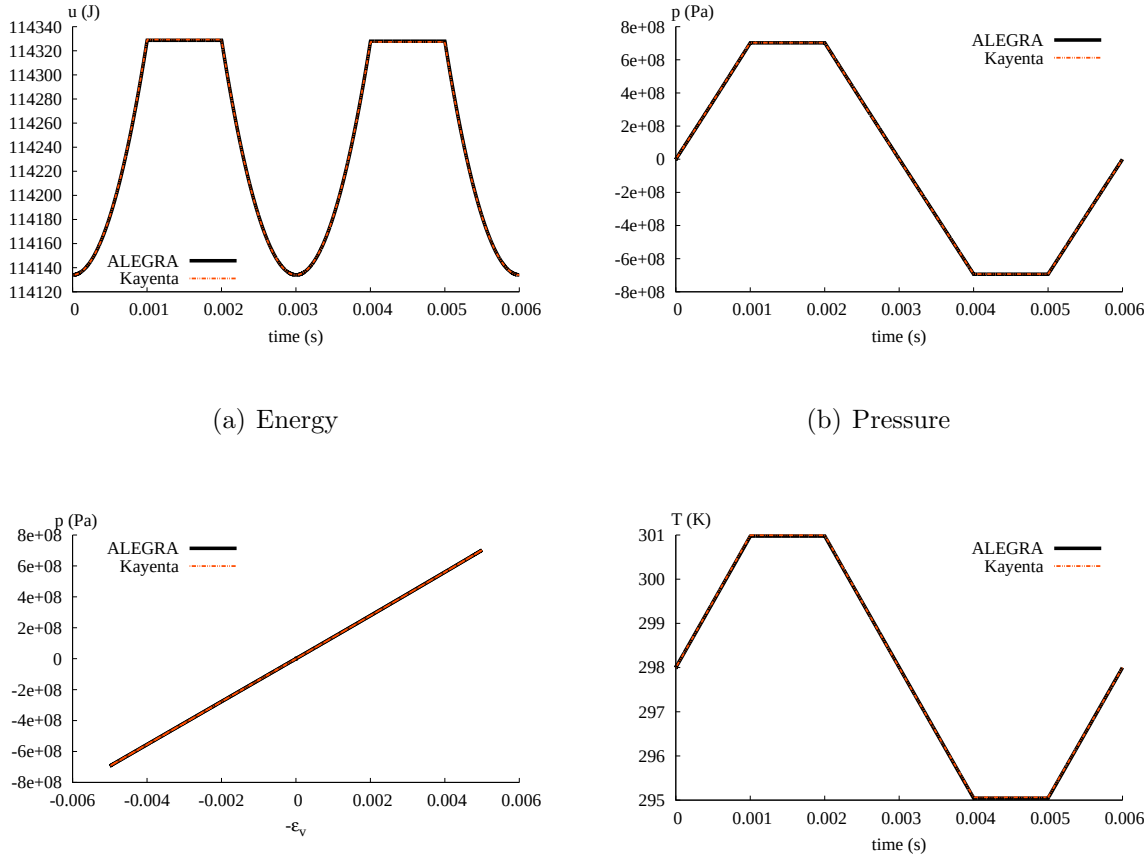

(a) Energy

(b) Pressure

(c) Pressure vs. Volumetric strain

(d) Temperature

Figure 6.2. Comparison of Thermo-Kayenta with ALEGRA for isotropic deformation.

The results, shown in Figure 6.2, show a high level of agreement between the two models, which is not surprising since both use identical Mie-Güneisen equation of state subroutines.

6.2 Case Study 2: Isochoric Deformation

In the previous comparisons, the response of the equation of state dominated the material response because of the isotropic nature of the deformation. In the following comparisons, an isochoric deformation is compared and the strength model will dominate the results. Isochoric deformation is also a good indicator if the deviatoric energy is being updated properly. The following strain path was used in each simulation:

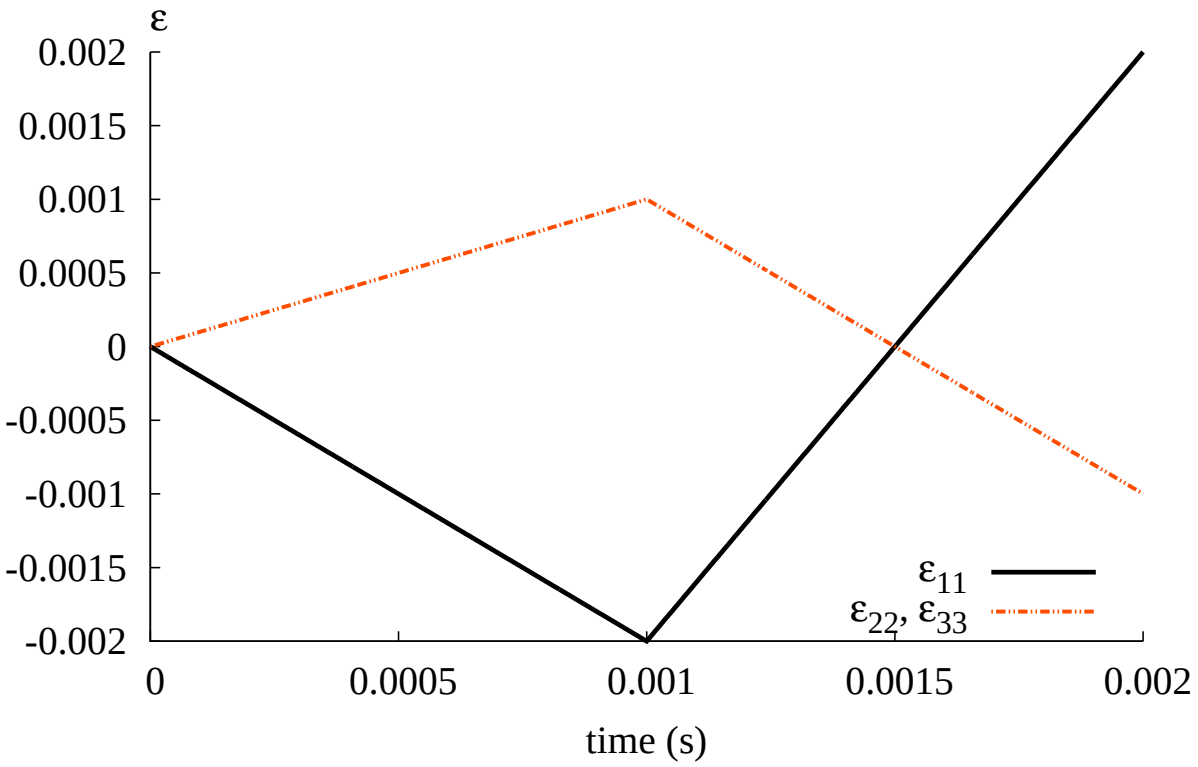

Figure 6.3. Prescribed isotropic strain path

In the following pages, the following features of Thermo-Kayenta will be compared with simulations run in ALEGRA through the same strain path. Each feature is enabled by adjusting the previously given parameters as indicated.

- Elastic response, $A = 10^{90}$ MPa
- Yield, $B = 0$ MPa, $C = 0$, $\theta_m = 10^{90}$ K

- Yield with thermal effects, $B = 0$ MPa, $C = 0$
- Yield with thermal and hardening effects, $C = 0$
- Yield with rate effects, $B = 0$ MPa, $\theta_m = 10^{90}$ K

We will begin, however, with a comparison of each of the separate features in Thermo-Kayenta.

Isochoric Deformation - Comparison of Different Features in Thermo-Kayenta

In Figure 6.4, hardening, thermal, and rate effects on yield in Thermo-Kayenta are compared.

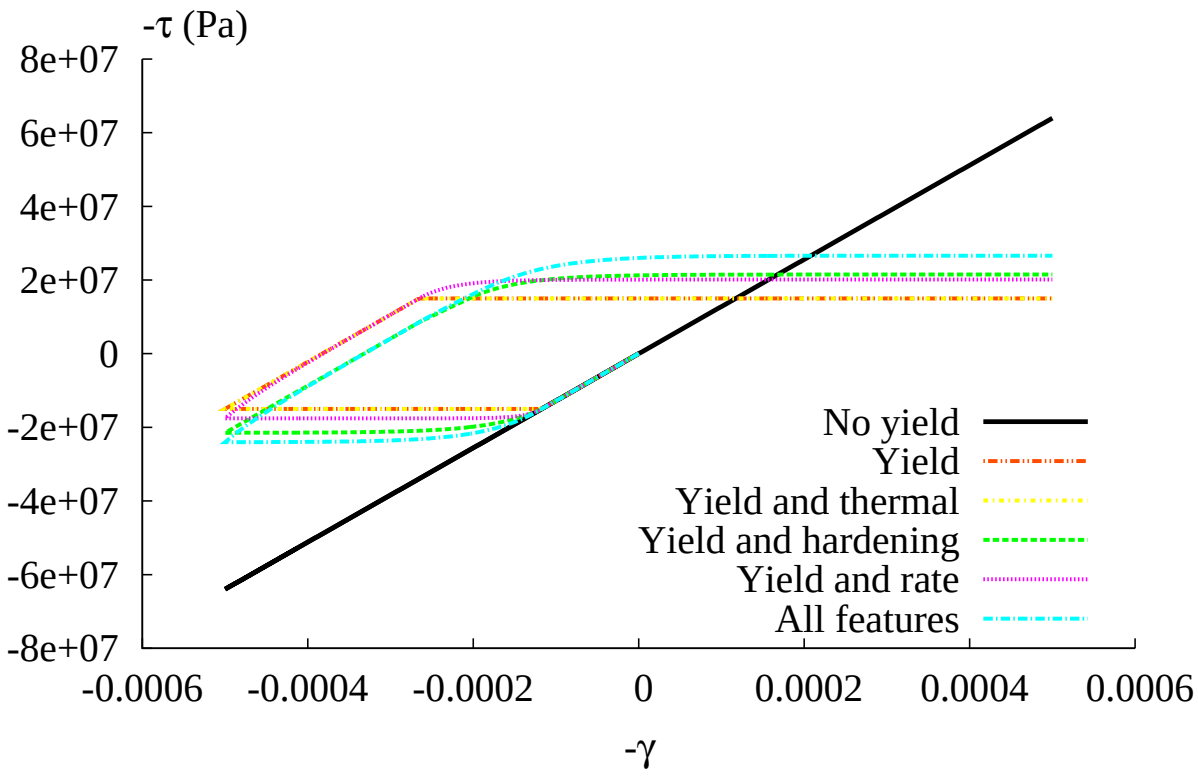

Figure 6.4. Comparison of features in Thermo-Kayenta for isochoric deformation.

The following trends are observed in Figure 6.4:

- Because of the limited final strain, the change in temperature is negligible for this simulation, thus, the difference between yield and yield with thermal effects is also negligible.
- When hardening is enabled, the strength of the material increases with plastic strain.

- When rate dependence is enabled, the apparent strength is higher than when not enabled.

Isochoric Deformation - Comparison of Elastic Response

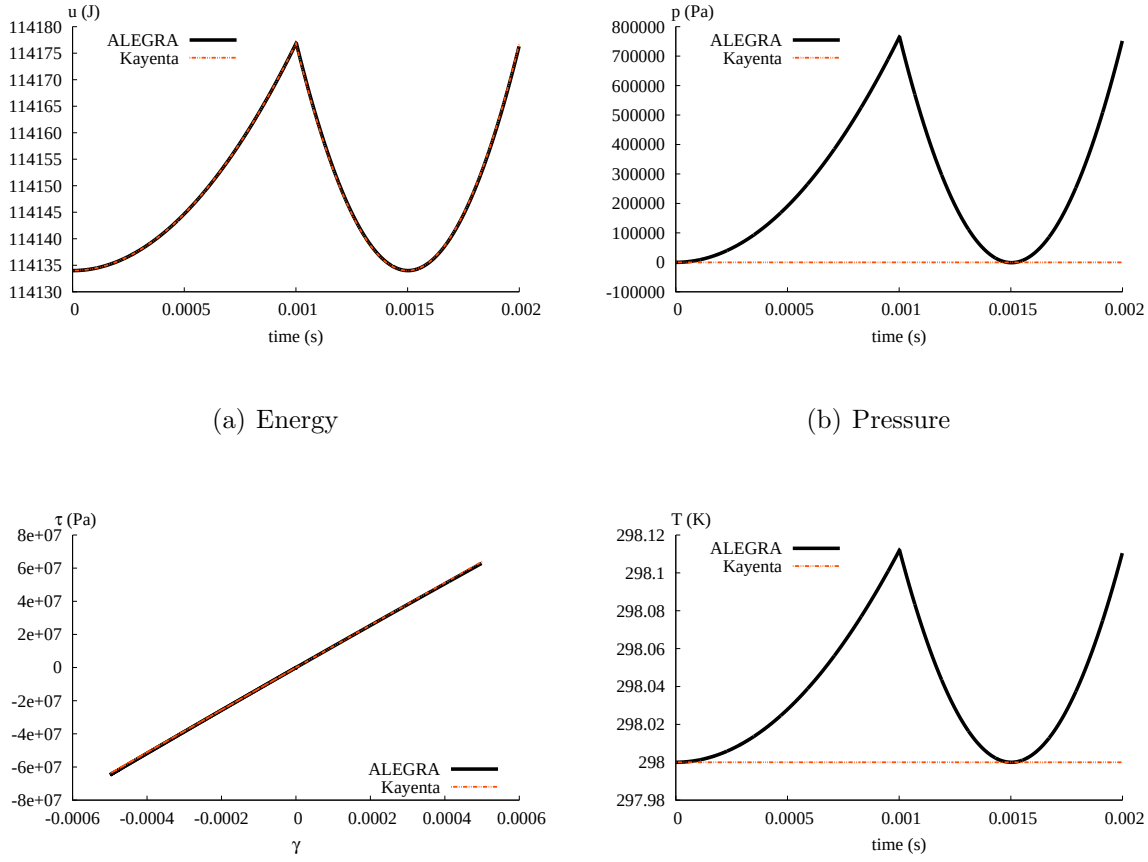

(a) Energy

(b) Pressure

(c) Maximum shear stress vs. shear strain

(d) Temperature

Figure 6.5. Comparison of the elastic response in Thermo-Kayenta with ALEGRA for isochoric deformation.

In these, and all of the plots of isochoric strain that follow, the non-negligible pressure in the ALEGRA simulations is due to the pressure being updated directly by the Mie-Güneisen equation of state, where pressure is allowed to vary with energy, even in the absence of volumetric strain. In Thermo-Kayenta, the pressure is updated according to $p = \kappa\varepsilon_v$, thus no pressure change is seen in the Thermo-Kayenta simulations. Similarly, in ALEGRA, the temperature is computed from the equation of state, whereas the temperature is computed from Eq. (4.14) in Thermo-Kayenta. With the exception of these two plots, all other quantities are in good agreement.

Isochoric Deformation - Comparison of Yield

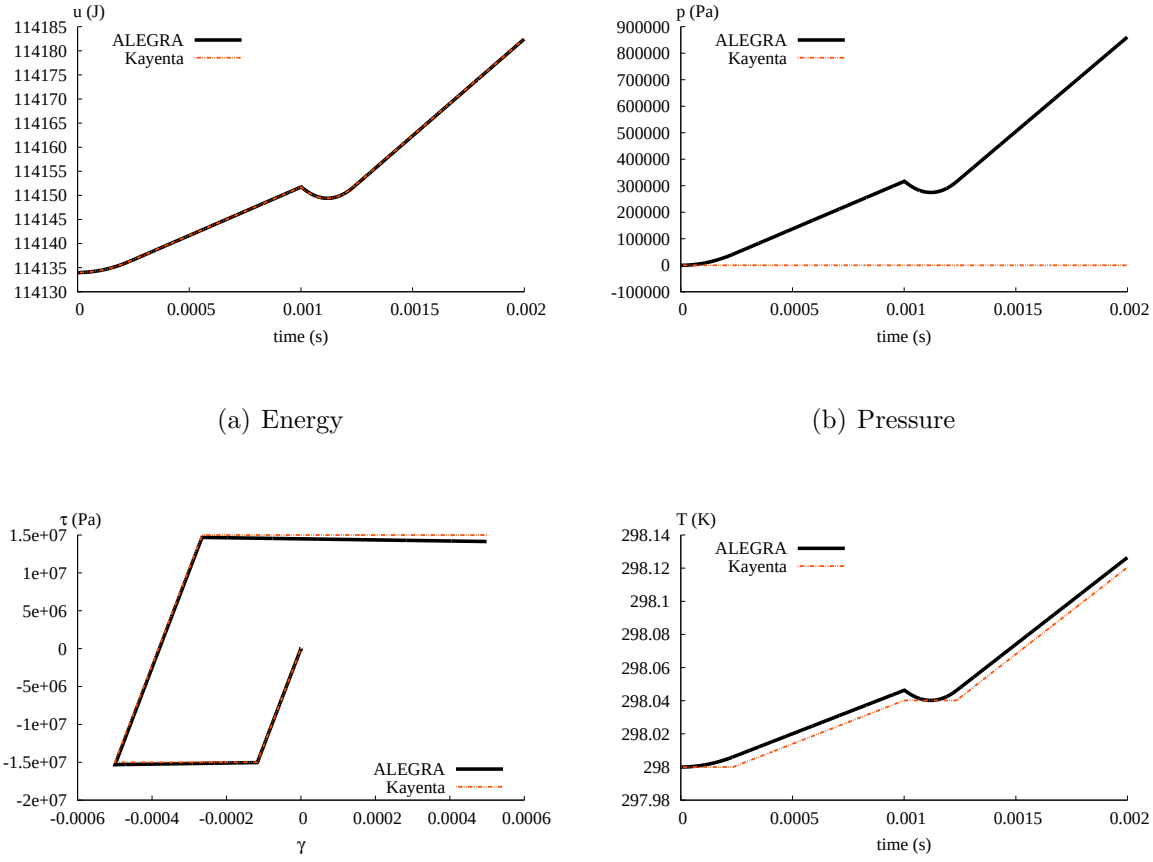

(a) Energy

(b) Pressure

(c) Maximum shear stress vs. shear strain

(d) Temperature

Figure 6.6. Comparison of the yield response in Thermo-Kayenta with ALEGRA for isochoric deformation.

Again, there is near perfect agreement between the two simulations, with the exception of the pressure and temperature plots, due to the reasons previously outlined. In the regions of plastic deformation, the temperatures in the two simulations increase identically, indicating that ALEGRA, like Thermo-Kayenta, converts 100% of plastic work to heat.

Isochoric Deformation - Comparison of Yield with Thermal Effects

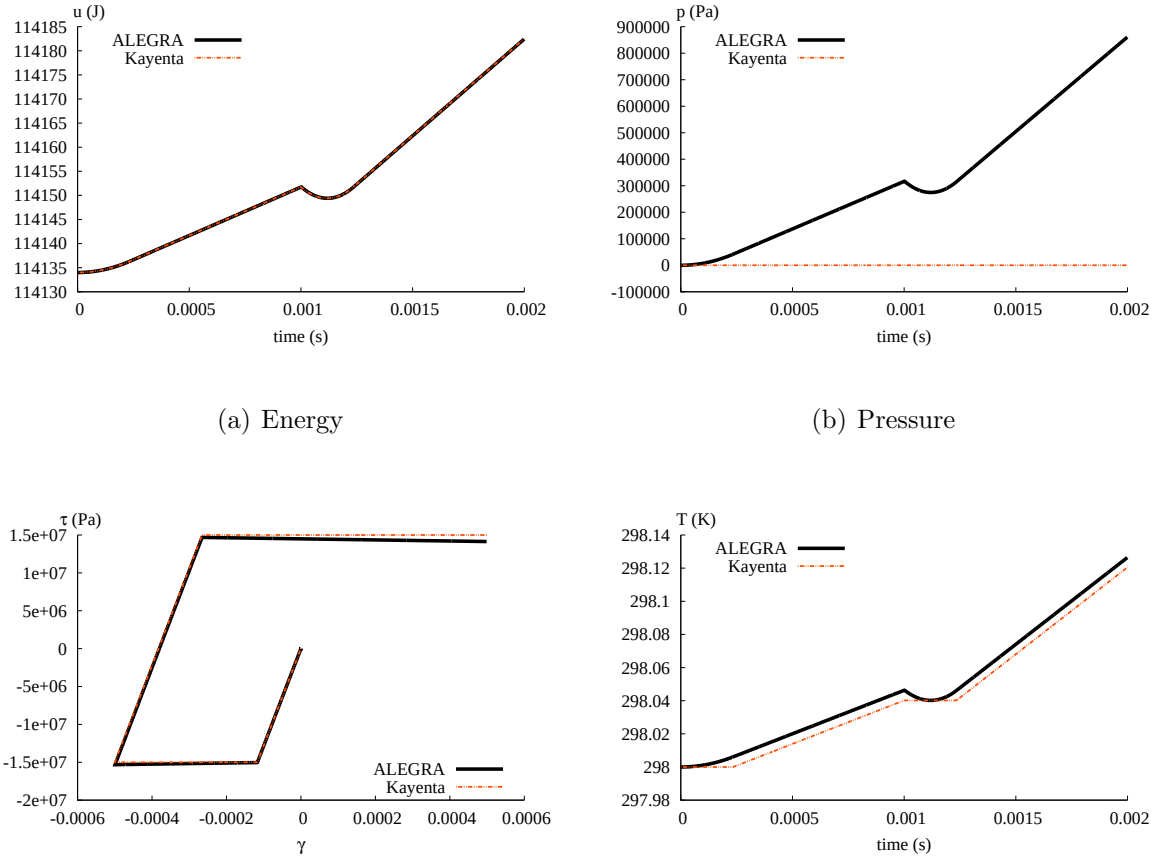

(a) Energy

(b) Pressure

(c) Maximum shear stress vs. shear strain

(d) Temperature

Figure 6.7. Comparison of Thermo-Kayenta with ALEGRA for isochoric deformation with yield and thermal effects enabled.

With thermal effects enabled, near perfect agreement is again obtained.

Isochoric Deformation - Comparison of Yield with Hardening

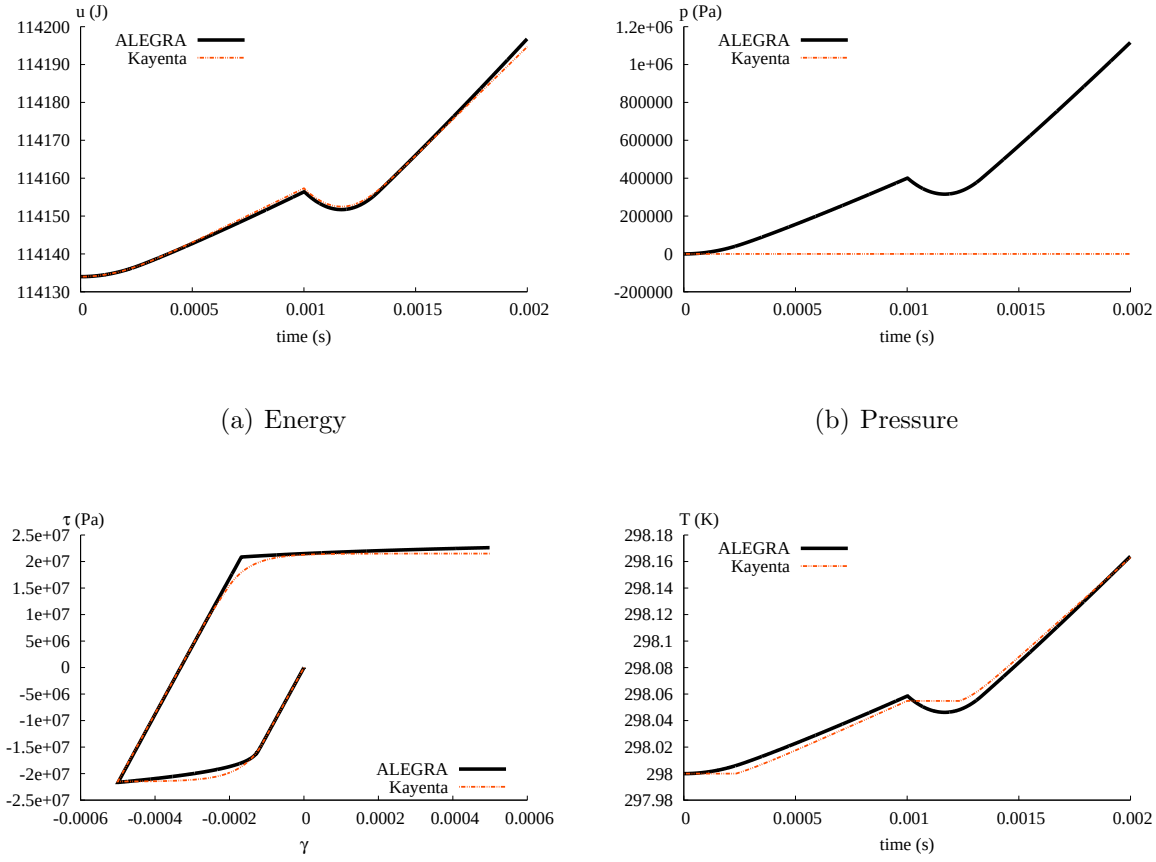

(a) Energy

(b) Pressure

(c) Maximum shear stress vs. shear strain

(d) Temperature

Figure 6.8. Comparison of Thermo-Kayenta with ALEGRA for isochoric deformation with yield and hardening effects enabled.

As in the previous isochoric simulations, the pressure and temperature results from ALEGRA are not agreement with those calculated from Thermo-Kayenta, due to reasons already described. In this simulation, however, there is also a discrepancy in the shear stress response. This is attributed to the difference in the implementation of material hardening in the two models. Because Thermo-Kayenta has its roots in modeling geological materials, the material is only allowed to harden to a limiting surface, at which points the hardening saturates. This behavior is responsible for the assymptoting stress response in Figure 6.8(c). In Johnson-Cook plasticity, the material is allowed to harden with plastic strain indefinitely. Power law hardening, which would allow for the stress state to harden beyond what is currently possible in Kayenta is currently being tested in Thermo-Kayenta.

Isochoric Deformation - Comparison of Yield with Rate Effects

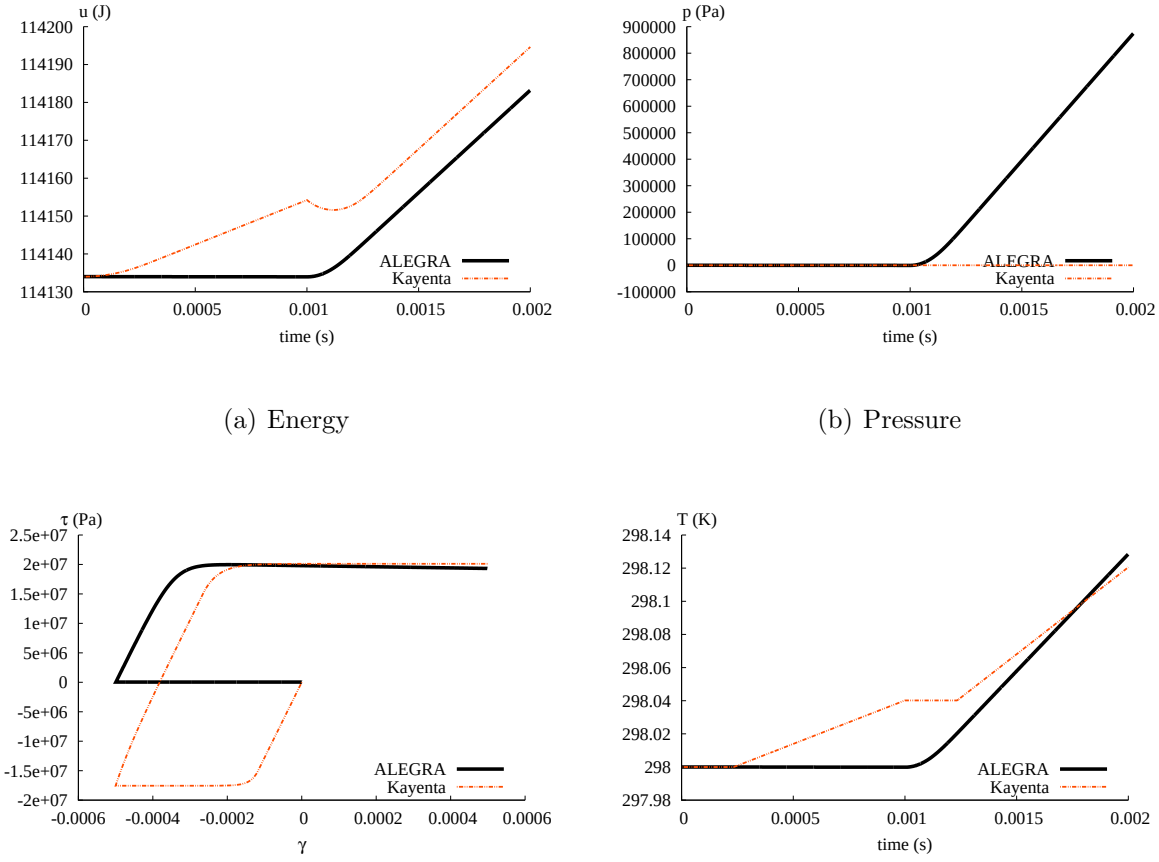

(a) Energy

(b) Pressure

(c) Maximum shear stress vs. shear strain

(d) Temperature

Figure 6.9. Comparison of Thermo-Kayenta with ALEGRA for isochoric deformation with yield and rate effects enabled.

With rate effects enabled in ALEGRA, plastic deformation commences immediately, resulting in much smaller values for energy, temperature, and axial stress than expected. Surprisingly, after unloading, the material response seems to correct itself and return to expected values. This behavior is due, in part, to the fact that the Johnson-Cook elastic-plastic model does not have a cutoff value for the strain rate, meaning that for strain rates less than one, the rate term, $(1 + C \ln \dot{\gamma}^*_{\text{eq}})$, can possibly return a negative value depending the value of C. In fact, if C is large enough, the negative rate term can cause the yield stress to vanish or become negative, which is what occurred in these simulations. A cutoff value for $\dot{\gamma}^*_{\text{eq}}$ of one will be implemented in future releases of ALEGRA to avoid this situation.

6.3 Case Study 3: Uniaxial Strain Deformation

Uniaxial strain is a good case study because it is neither purely isotropic nor isochoric. It is also a commonly encountered strain path in shock and plate impact experiments. The following strain path was used in each simulation:

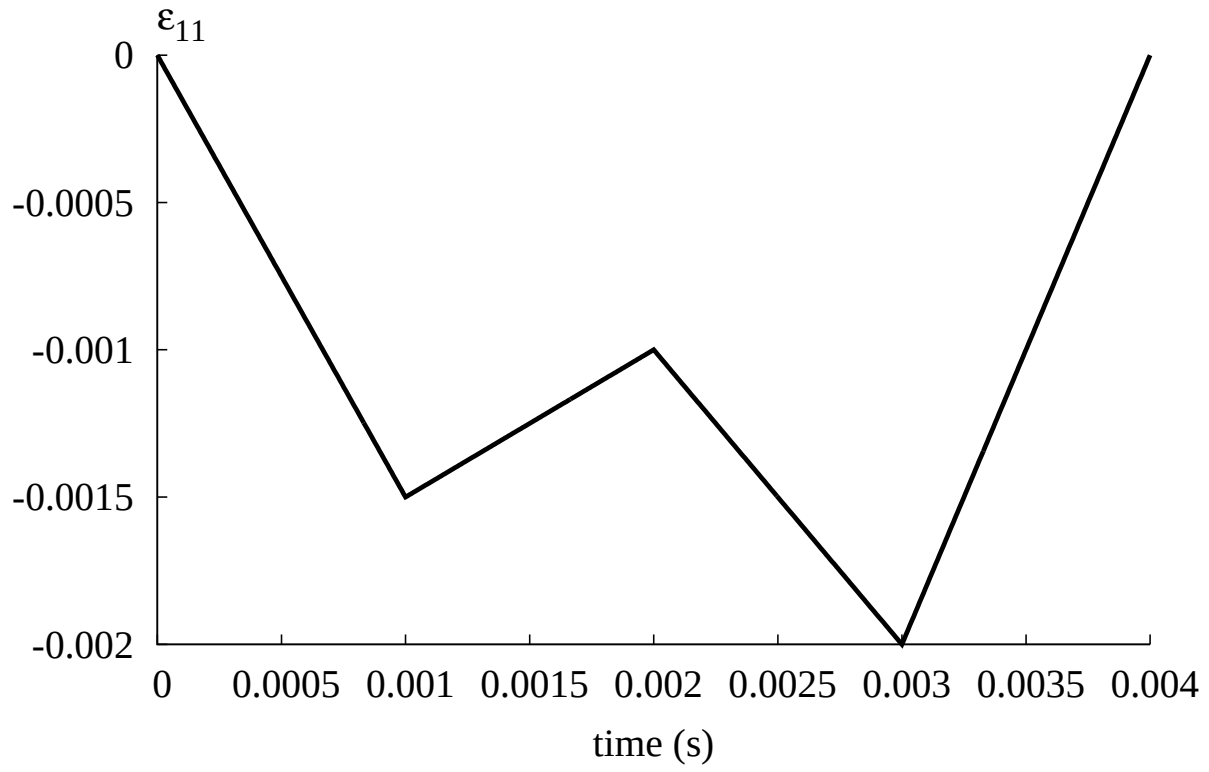

Figure 6.10. Prescribed uniaxial strain path

We will begin again by comparing the material response with the different features of Thermo-Kayenta enabled.

Uniaxial Strain Deformation - Comparison of different features in Thermo-Kayenta

In Figure 6.11, effects of hardening, thermal, and rate effects on yield in Thermo-Kayenta are compared.

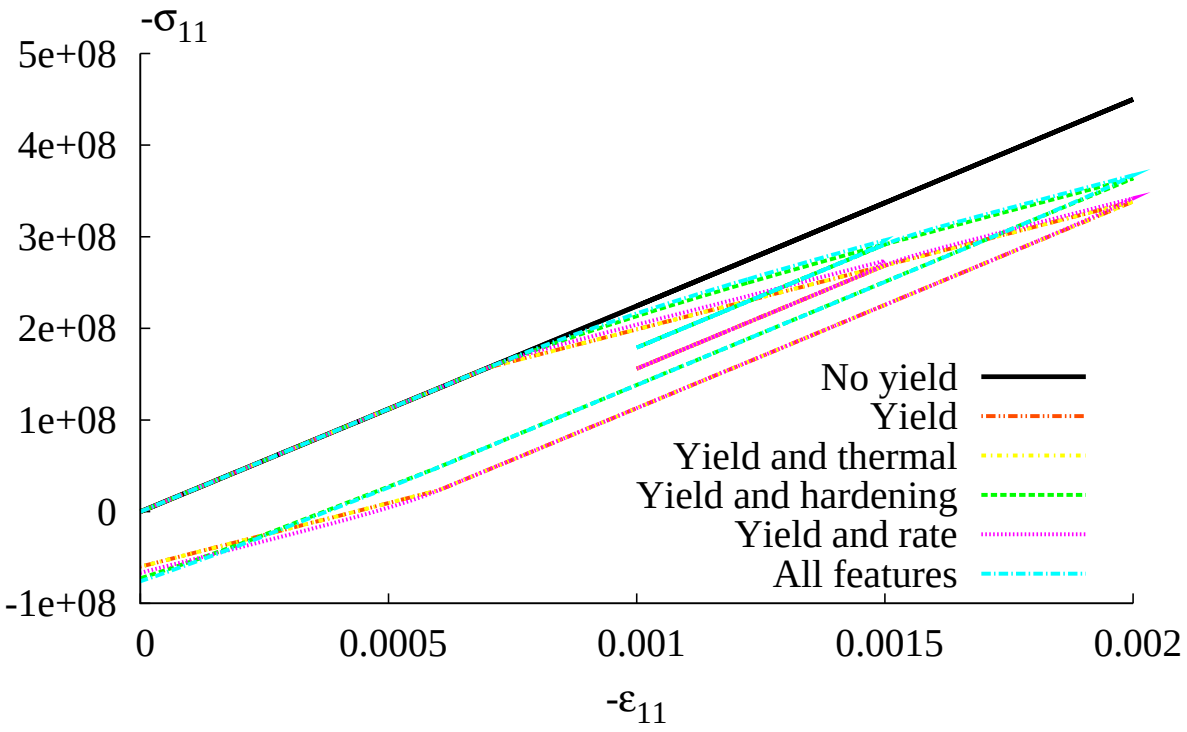

Figure 6.11. Comparison of features in Thermo-Kayenta for uniaxial strain deformation.

Uniaxial Strain Deformation - Elastic Response

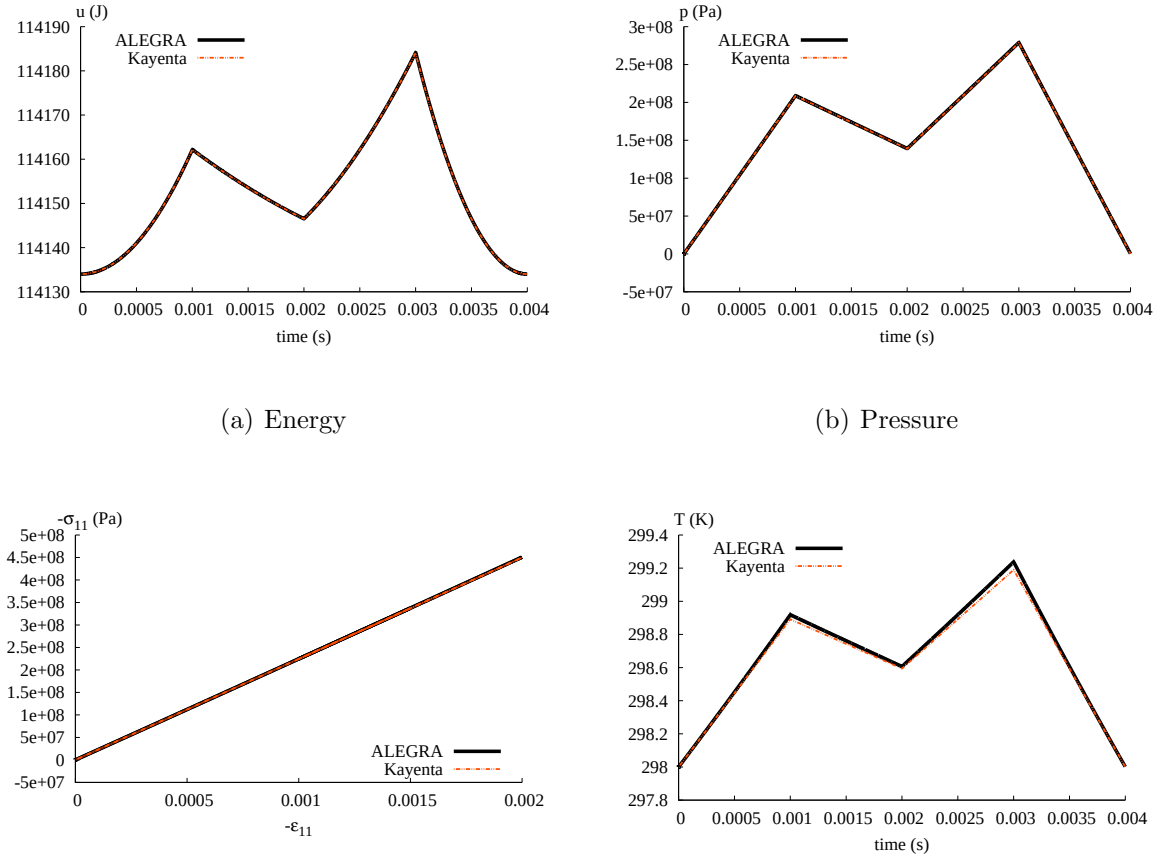

(a) Energy

(b) Pressure

(c) Stress-Strain

(d) Temperature

Figure 6.12. Comparison of the elastic response in Thermo-Kayenta with ALEGRA for uniaxial deformation.

The elastic response in both models is in near perfect agreement between Thermo-Kayenta and ALEGRA's Johnson-Cook model.

Uniaxial Strain Deformation - Comparison of Yield

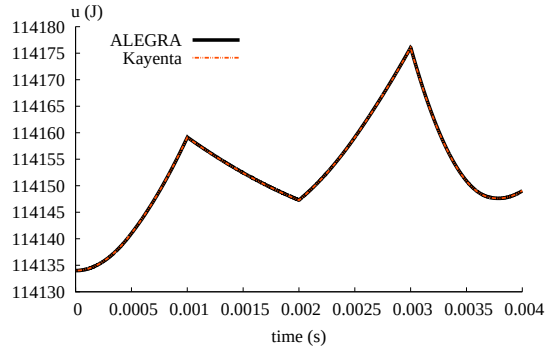

(a) Energy

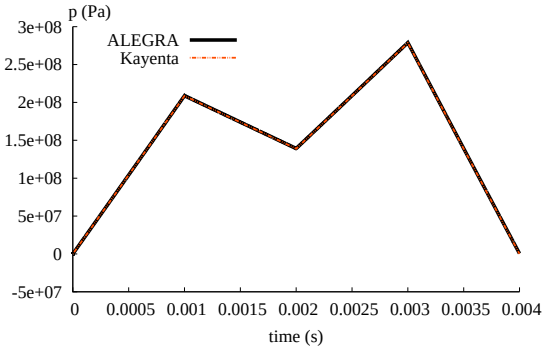

(b) Pressure

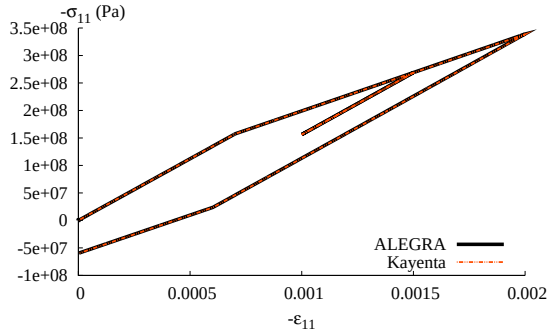

(c) Stress-Strain

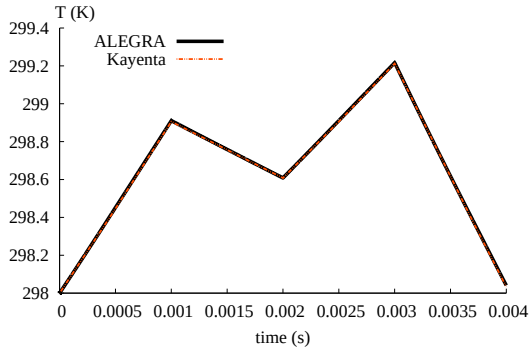

(d) Temperature

Figure 6.13. Comparison of Thermo-Kayenta with ALEGRA for uniaxial strain deformation with yield enabled.

Again, in this simulation the results are in near perfect agreement.

Uniaxial Strain Deformation - Comparison of Yield with Thermal Effects

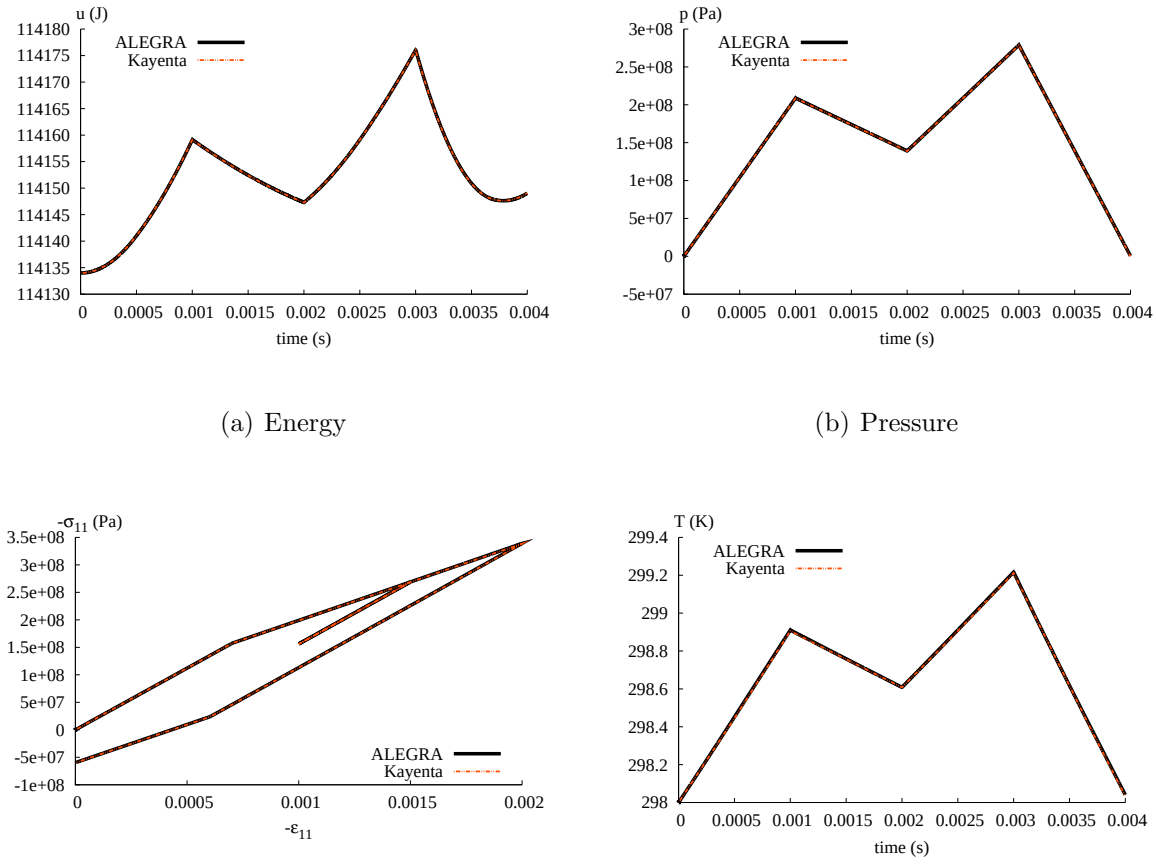

(a) Energy

(b) Pressure

(c) Stress-Strain

(d) Temperature

Figure 6.14. Comparison of Thermo-Kayenta with ALEGRA for isochoric deformation with yield and thermal effects enabled.

Because of the limited strain in this case study, the temperature increases very little. Thus, the thermal effects on yield are negligible. Again, as in the previous case (yield enabled), the results seem to be in near perfect agreement.

Uniaxial Strain Deformation - Comparison of Yield with Hardening

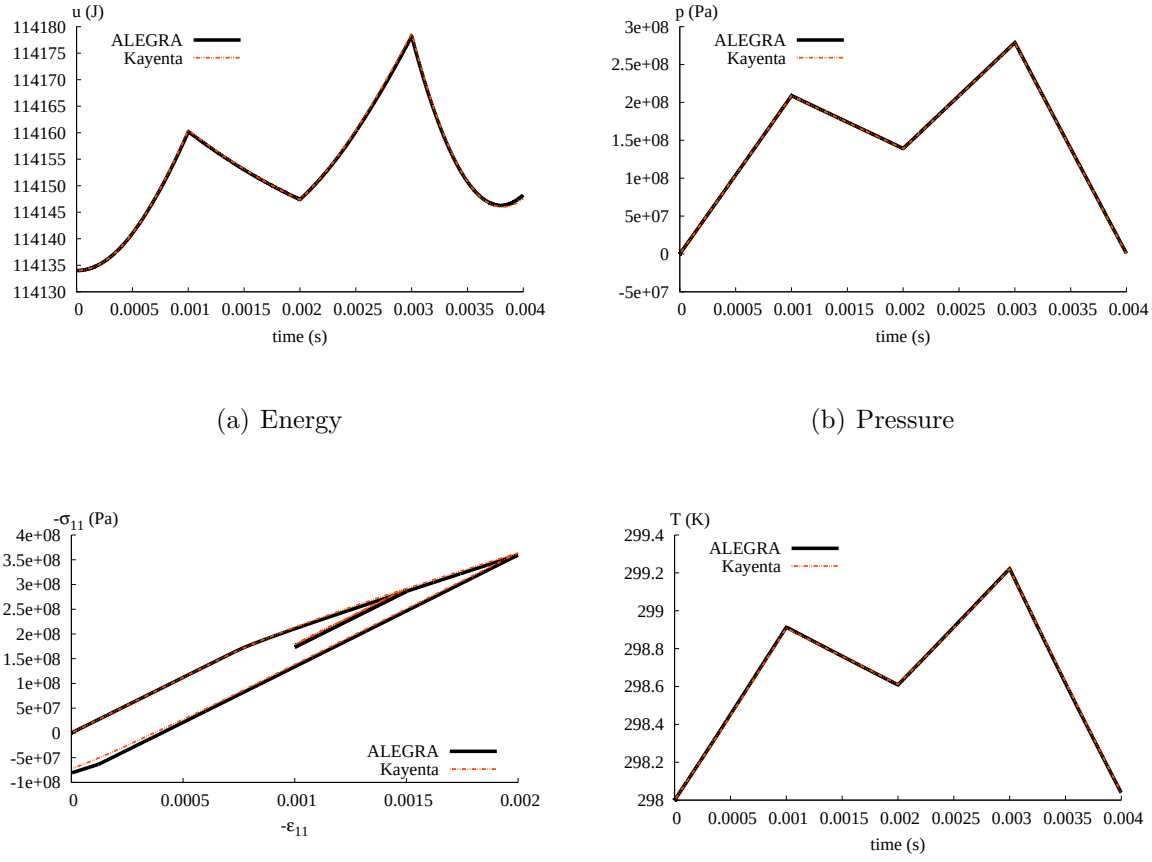

(a) Energy

(b) Pressure

(c) Stress-Strain

(d) Temperature

Figure 6.15. Comparison of Thermo-Kayenta with ALEGRA for uniaxial strain deformation with yield and hardening effects enabled.

Again, the results are in near perfect agreement, with the exception of the axial stress response on the unloading leg. The difference in the stress level is attributed to the hardening schemes employed by the two models. Thermo-Kayenta employs kinematic hardening while the Johnson-Cook model employs isotropic hardening. The difference in the two types of hardening schemes is evident at the point where plastic deformation commences in the *unloading* leg. With isotropic hardening, the yield surface expands in size allowing the realizations of stress states not initially achievable in both the loading and *unloading* legs. Kinematic hardening, on the other hand, entails a kinematic *shift* in the yield surface, allowing initially unachievable stress states in the loading leg, but not in the unloading leg, unless further plastic loading in the unloading direction shifts the yield surface in that direction.

Uniaxial Strain Deformation - Comparison of Yield with Rate Effects

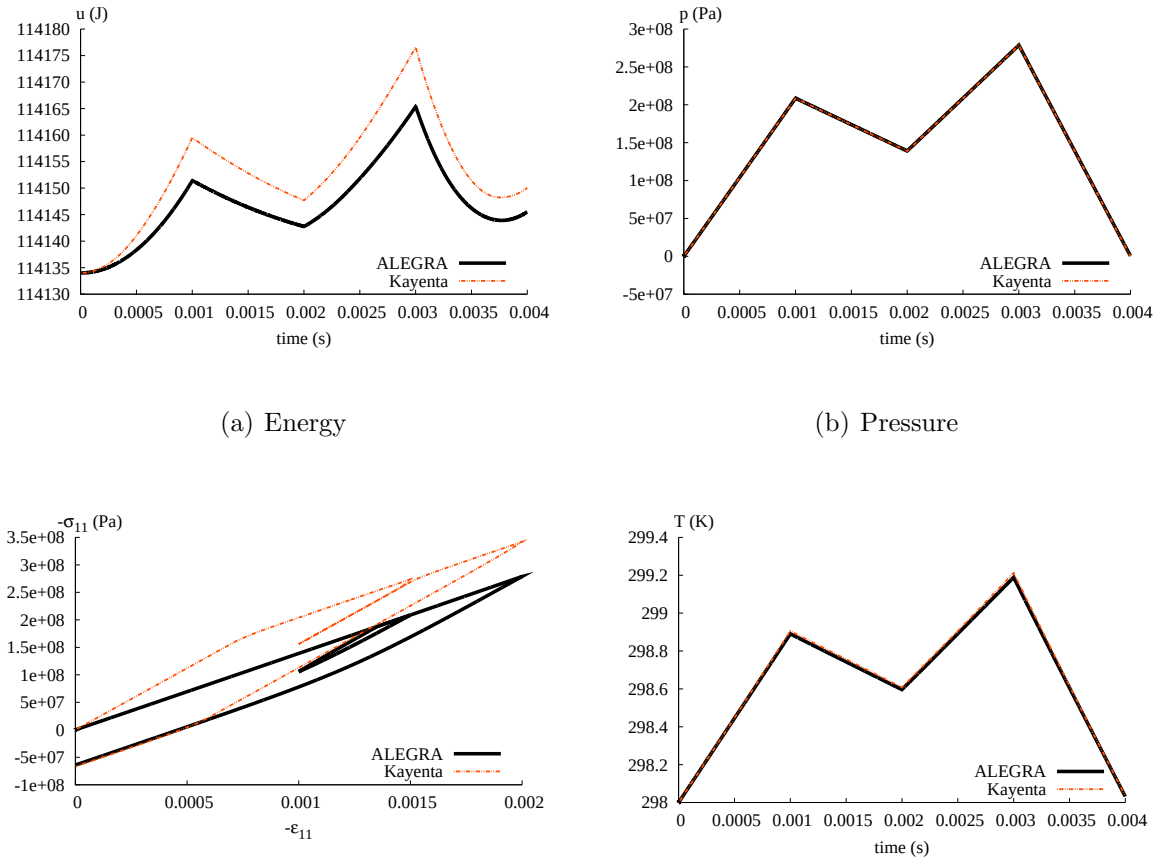

(a) Energy

(b) Pressure

(c) Stress-Strain

(d) Temperature

Figure 6.16. Comparison of Thermo-Kayenta with ALEGRA for isochoric deformation with yield and rate effects enabled.

With rate effects enabled in ALEGRA's installation of Johnson-Cook, the material yields almost immediately, as previously discussed. Thus, the axial stress response is not in agreement between the two simulations. The difference in axial response is directly responsible for the difference in energy.

6.4 Case Study 4: Taylor Impact

Thermo-Kayenta was installed in LS-Dyna and Taylor impact simulations were performed. The following plots compare the results from Thermo-Kayenta with LS-Dyna's built in Johnson-Cook using LS-Dyna's Mie-Güneisenequation of state for identical simulations. The results of each are compared against experimental data measured by Wilkins and Guinan [19]. The following data were used for each simulation:

Material	Copper
Initial temperature	298 K
Initial length	23.47 mm
Initial diameter	7.62 mm
Impact velocity	210 m/s
Physical time simulated	100 μs

Table 6.4. Data used in for Taylor impact simulations performed in LS-Dyna

Results

Comparisons of the results from the end of the simulations using Thermo-Kayenta with Johnson-Cook and experimental data are shown in Figures 6.17–6.19. In Figure 6.17, temperature contours for Thermo-Kayenta and a comparison of the displacement profile with experimental data are shown. In Figures 6.18 and 6.19, displacement profiles and temperature contours from Thermo-Kayenta and Johnson-Cook are compared.

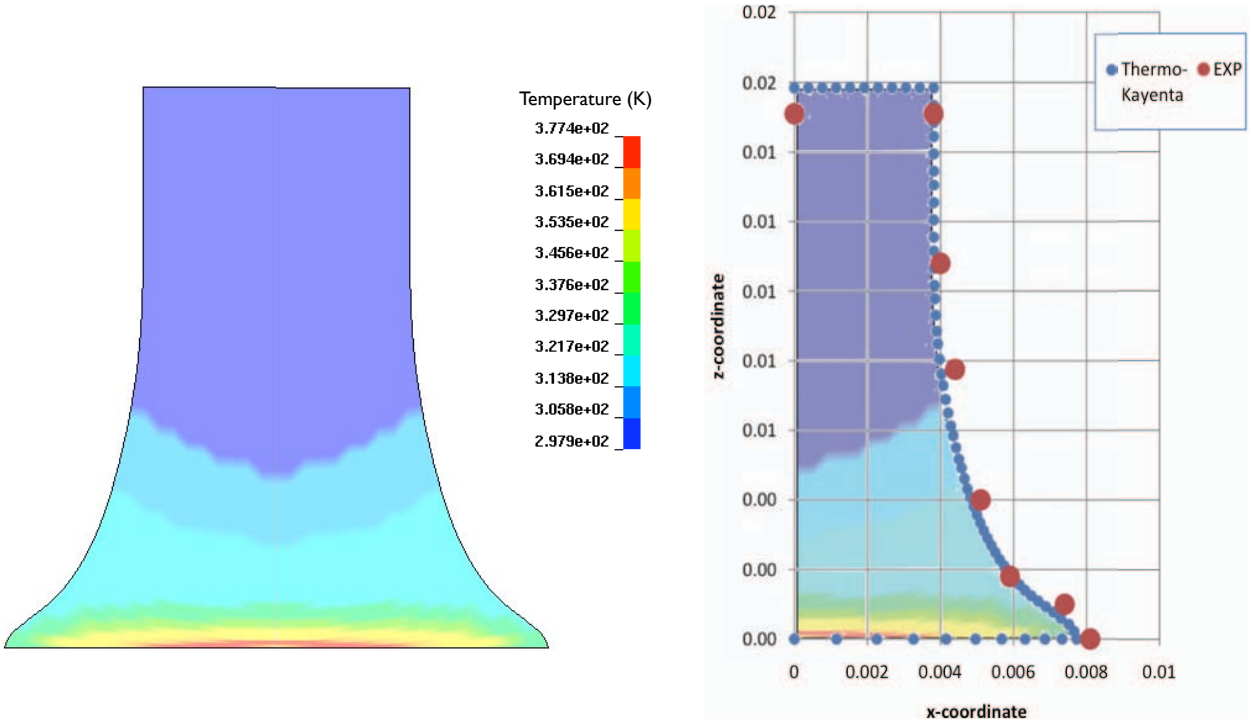

Figure 6.17. Displacement profile for Thermo-Kayenta at the end of the simulation. The red dots represent the experimental profiles as given in [19].

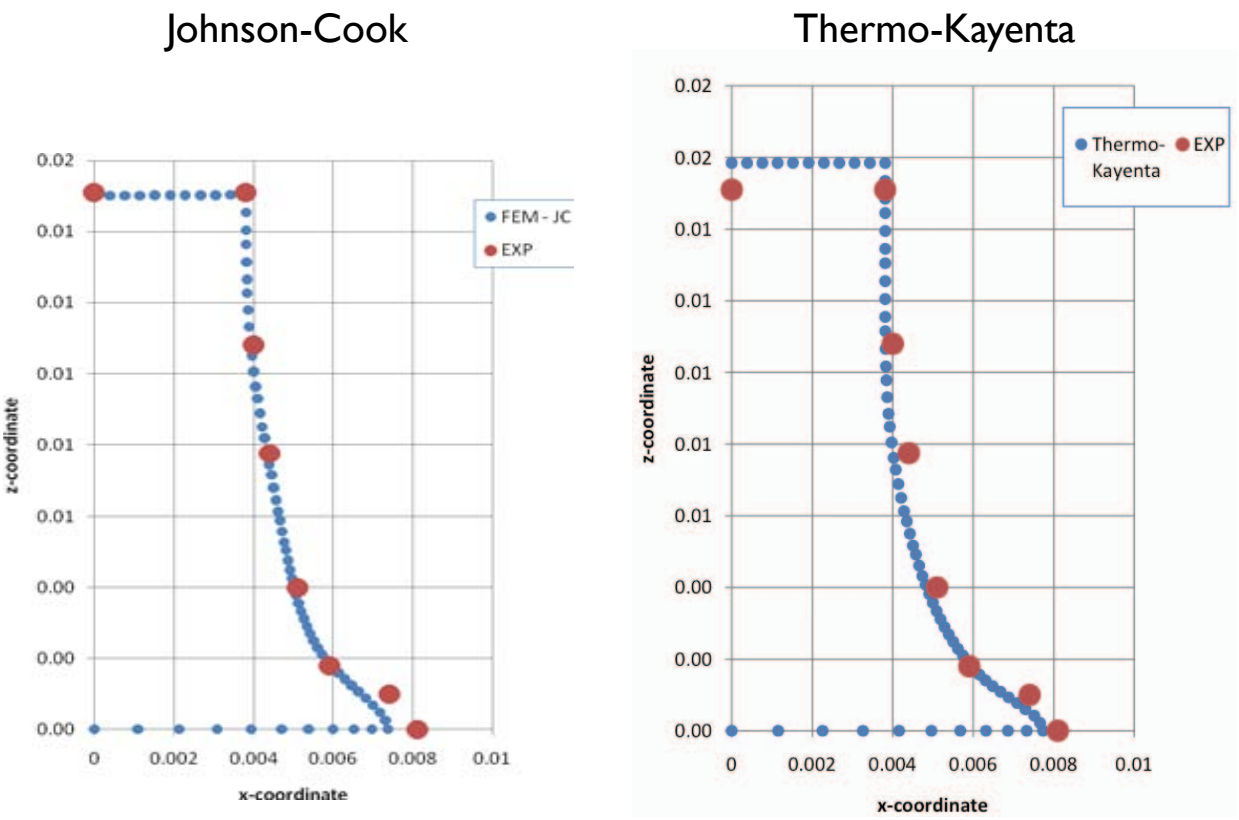

Figure 6.18. Comparison of the displacement profile for Thermo-Kayenta and Johnson-Cook. The red dots in each plot represent the experimental profiles as given in [19].

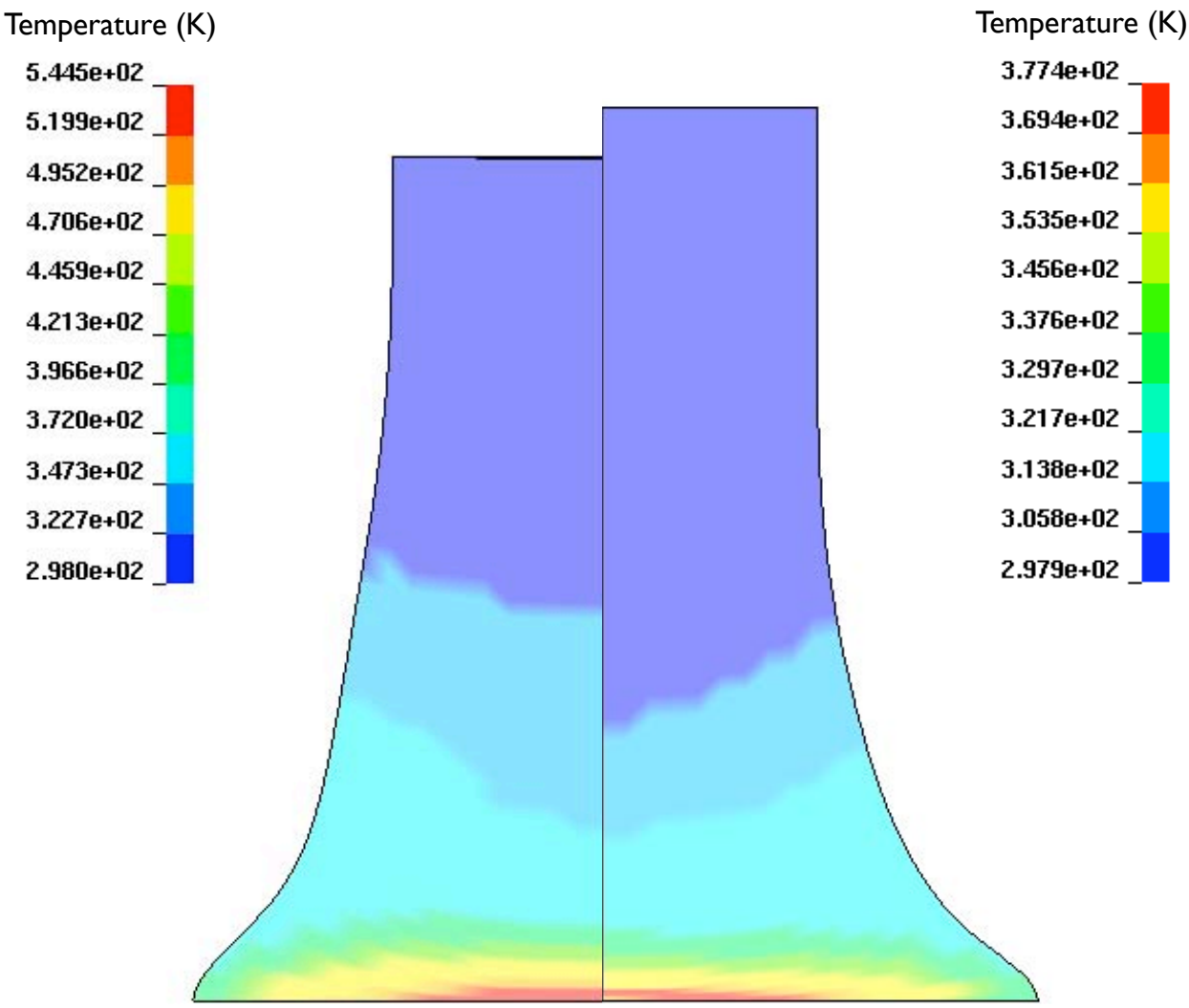

Figure 6.19. Comparison of the temperature contours for Thermo-Kayenta and Johnson-Cook.

While the discrepancy in the height and width of the deformed profile is not significant between the two simulations, the discrepancy in the peak temperature ($\approx 31\%$) is. The source of the discrepancies is most likely related to the limiting value placed on the stress due to the hardening scheme in Thermo-Kayenta. Since $\theta \propto \boldsymbol{\tau} : \dot{\boldsymbol{\varepsilon}}$, it is expected that the temperature will be lower in the Thermo-Kayenta simulations as the stress reaches this limiting value. When the hardening scheme in Kayenta is adjusted to allow for power law type hardening we expect the temperature levels to be in better agreement.

Chapter 7

Conclusion

To extend the capabilities of Kayenta to include metals, the Computational Solid Mechanics (CSM) group at the University of Utah has modified Kayenta to include thermal response due to deformation. This new version of Kayenta, dubbed Thermo-Kayenta, is capable of reproducing single-element response curves for the Johnson-Cook thermoplasticity model [4] with the Mie-Gruneissen EOS under strain-controlled compression, pure shear, and uniaxial strain. The target response functions (stress and temperature as functions of time) were provided by SNL. Thermo-Kayenta was also shown to give very satisfactory results in Taylor impact simulations performed in LS-Dyna.

Like most thermoplastic models developed for use in shock loading, the equations solved by Thermo-Kayenta were derived based on the assumption of adiabatic loading. Unlike most of those other models, however, Thermo-Kayenta tracks the evolving thermal state internally, requiring no more additional information at each timestep than the non-thermal versions of Kayenta. The advantages of tracking the evolving thermal state internally are twofold: 1) Installation of Thermo-Kayenta in host codes which already have Kayenta installed, requires little more than providing additional thermal parameters to the user input array. 2) The thermomechanical equations are solved in a consistent manner.

Though Thermo-Kayenta can be shown to reduce to the classical Johnson-Cook thermoplastic model, there are several outstanding issues that should be resolved for Thermo-Kayenta to be considered thermodynamically consistent. These issues include, properly evolving temperature with the changing material state, using a consistent consistency parameter, and inclusion of deformation induced, reversible anisotropy, among others. At the core of each of these issues is the lack of a functional form of the internal energy in Thermo-Kayenta (Thermo-Kayenta is a hypo-elastic model).

Despite the current inconsistencies with thermodynamics, the initial inclusion of thermodynamics in Kayenta is a step in the right direction of creating a thermodynamically consistent model. In its current form, it is capable of reducing to linear elasticity, linear-thermoelasticity, classical plasticity theories, and classical Johnson-Cook thermoplasticity, in addition to more sophisticated plasticity theories. Thermo-Kayenta accomplishes all of this while remaining, at its core, a phenomenological engineering model; meaning, parameters required by the model are attainable through standard macroscopic experiments. Finally, Thermo-Kayenta is a very tractable model and easily installed in *any* host code that is capable of calling external FORTRAN material models.

References

[1] A. Fossum and R. Brannon, "THE SANDIA GEOMODEL: Theory and user's guide," Tech. Rep. SAND2004-3226, Sandia National Laboratory, 2005.

[2] R. Brannon, A. Fossum, and O. Strack, "Kayenta: Theory and User's Guide," Tech. Rep. SAND2009-2282, Sandia National Laboratory, 2009.

[3] J. Lubliner, *Plasticity Theory*. Dover Publications, 2008.

[4] G. Johnson and W. Cook, "A constitutive model and data for metal subjected to large strains, high strain rates, and high temperatures," in 7^{th} *International Symposium on Ballisitics*, pp. 541–547, 1985.

[5] L. Malvern, *An Introduction to the Mechanics of a Continuous Medium*. Prentice-Hall Inc., 1969.

[6] C. Truesdell, W. Noll, and S. S. Antman, *The non-linear field theories of mechanics*, vol. 3. Springer, 2004.

[7] P. M. Helnwein, "Some remarks on the compressed matrix representation of symmetric second-order and fourth-order tensors," *Comp Meth Appl Mech Eng*, vol. 190, pp. 2753–2770, 2001.

[8] D. Drumheller, *Introduction to Wave Propogation in Nonlinear Fluids and Solids*. Cambridge University Press, 1998.

[9] A. Hoger, "The material time derivative of logarithmic strain," *Int J Sol Struct*, vol. 22, no. 9, pp. 1019–1032, 1986.

[10] T. Wright, *The Physics and Mathematics of Adiabatic Shear Bands*. Cambridge University Press, 2002.

[11] P. Rosakis, A. Rosakis, G. Ravichandran, and J. Hodowany, "A thermodynamic internal variable model for the partition of plastic work into heat and stored energy in metals," *J Mech Phys Sol*, vol. 48, pp. 581–607, 2000.

[12] R. M. Brannon, "Elements of phenomenological plasticity: Geometrical insight, computational algorithms, and topics in shock physics," in *Shock Wave Science and Technology Reference Library* (Y. Horie, ed.), vol. 2, pp. 225–274, Springer Berlin, 2007.

[13] G. Taylor and H. Quinney, "The latent energy remaining in a metal after cold working," *Proc Roy Soc Lon A*, vol. 143, no. 849, pp. 307–326, 1934.

[14] G. Duvaut and J. Lions, *Inequalities in mechanics and physics*, vol. 219. Springer Berlin, 1976.

[15] G. Johnson and W. Arnold, "Fracture characteristics of three metals subjected to various strains, strain rates, temperatures and pressures," *Int J Eng Frac Mech*, vol. 21, pp. 31–48, 1985.

[16] J. Simo and T. Hughes, *Computational Inelasticity*. Springer, 2000.

[17] B. Banerjee, "An evaluation of plastic flow stress models for the simulation of high-temperature and high-strain-rate deformation of metals." Submitted to Elsevier, http://www.eng.utah.edu/ banerjee/Papers/CuPlasticCompare.pdf, 2005.

[18] R. Brannon and M. Wong, "Mig 0.0 model interface guidelines: Rules to accelerate installation of numerical models into any compliant parent code," Tech. Rep. SAND96-2000 UC-405, Sandia National Laboratory, 1996.

[19] M. Wilkins and M. Guinan, "Impact of cylinders on a rigid body," *J Appl Phys*, vol. 44, no. 3, pp. 1200–1206, 1973.

$\boldsymbol{a}$	Material acceleration, $\ddot{\boldsymbol{x}}$, page 14
$\boldsymbol{b}$	Body force per unit mass, page 14
$\partial\Omega$	Boundary of domain Ω, page 14
$\boldsymbol{\alpha}$	Backstress tensor, page 25
$\boldsymbol{\Lambda}$	Elastic-plastic coupling tensor, page 21
$\dot{\boldsymbol{\gamma}}^{\mathrm{p}}$	Deviatoric part of the plastic strain rate, page 26
ρ	Material density, page 14
$\dot{\gamma}^{*}_{\mathrm{eq}}$	Normalized plastic strain rate used in Johnson-Cook plasticity, page 26
$\mathcal{D}$	Internal dissipation, $\mathcal{D} = J\boldsymbol{\sigma}\!:\!\boldsymbol{d} + \rho_0\theta\dot{s} - \dot{u}$, page 16
$\dot{\boldsymbol{\varepsilon}}^{\mathrm{e}}$	Elastic strain rate, page 18
$\dot{\boldsymbol{\varepsilon}}^{\mathrm{p}}$	Plastic strain rate, page 20
Ω	An enclosed domain, page 14
r	Energy production per unit mass, page 14
u	Internal energy per unit reference volume, page 14
u_c	Cold energy, page 27
u_θ	Thermal energy, page 27
H	Ensemble hardening modulus,$H = -\dfrac{\partial f/\partial q_k}{\|\partial f/\partial \boldsymbol{\tau}\|}h_k$, page 21
S	Total entropy of the system, page 15
s	Specific entropy of the system, page 15
γ_{eq}	Equivalent plastic strain, page 26
$\boldsymbol{m}$	Direction of plastic flow., page 20
$\boldsymbol{\Gamma}$	Grüneisen tensor, $\boldsymbol{\Gamma} = -\dfrac{1}{\rho_0\theta}\dfrac{\partial \boldsymbol{\tau}}{\partial s}$, page 17
$\boldsymbol{\mathcal{V}}$	General strain measure, page 16
$\boldsymbol{\mathcal{P}}$	General stress measure, page 16

$\boldsymbol{q}$ Heat flux vector, page 14

$\mathbb{C}_s$ Isentropic elastic stiffness tensor, $\mathbb{C} = \dfrac{\partial^2 u}{\partial \boldsymbol{\varepsilon} \partial \boldsymbol{\varepsilon}}$, page 17

q_k Internal variables that change with dissipation, page 18

θ_0 Reference temperature used in Johnson-Cook plasticity, page 26

$\dot{\lambda}$ Magnitude of the plastic strain rate., page 20

$\boldsymbol{n}$ Outward unit normal of $\partial\Omega$, page 14

p Equilibrium pressure, $p = -\dfrac{\partial u}{\partial V}$, page 28

$\mathcal{F}$ Heat conductive dissipation, $\mathcal{F} = -\dfrac{J}{\theta}\boldsymbol{q} \bullet \vec{\nabla}\theta$, page 16

$\boldsymbol{p}$ Plastic return direction, page 21

$\boldsymbol{\xi}$ Shifted stress tensor, $\boldsymbol{\xi} = \boldsymbol{\sigma} - \boldsymbol{\alpha}$, page 25

c_v Specific heat at constant volume, $c_v = \dfrac{\theta}{\partial\theta/\partial s}$, page 17

$\mathbb{C}$ Isothermal stiffness tensor, $\mathbb{C} = \mathbb{C}_s - \rho_0 \theta c_v \boldsymbol{\Gamma}\boldsymbol{\Gamma}$, page 18

$\boldsymbol{\sigma}$ Cauchy stress tensor, page 14

$\boldsymbol{d}$ Symmetric part of the velocity gradient, sym $\boldsymbol{L}$, page 14

θ Absolute temperature, page 15

θ^* Normalized temperature used in Johnson-Cook plasticity, page 26

θ_{m} Melt temperature, page 26

Θ Temperature modulus $\Theta = -\dfrac{\partial f/\partial\theta}{\|\partial f/\partial \boldsymbol{\tau}\|}$, page 21

P_θ Correction to trial temperature increment, page 21

m User specified exponent in the temperature term of Thermo-Kayenta's yield condition, page 31

χ Taylor-Quinney coefficient of plastic work converted to heat, page 23

$\boldsymbol{v}$ Material velocity, $\dot{\boldsymbol{x}}$, page 14

v_n Velocity normal to $\partial\Omega$, page 14

V Specific volume, page 28

A, B, C, n, m	Material constants used in Johnson-Cook plasticity model, page 26
H	Material constant associated with kinematic hardening, page 26
$\dot{\gamma}_0$	User defined plastic strain-rate used in Johnson-Cook plasticity, page 26
$\mathbf{E}_i$	Orthonormal Cartesion unit basis tensor in $\mathbb{R}^6$, page 13
$\mathbf{e}_i$	Orthonormal Cartesion unit basis tensor in $\mathbb{R}^3$, page 13
$\mathbb{R}^n$	Set of real numbers in n dimensional space, page 13

DISTRIBUTION:

1 MS 0899 Technical Library, 9536 (electronic)

Sandia National Laboratories